Study of a Model Fermi Liquid Interacting via a Hard-core Repulsive Potential and an Attractive Tail*

by

Tai Kai Ng
Department of Physics and Astronomy
Northwestern University
Evanston, IL 60201

and

K. S. Singwi
Department of Physics and Astronomy
Northwestern University
and
Materials Science and Technology Division
ARGONNE NATIONAL LABORATORY
Argonne, IL 60439

ANL/PPRNT--89-121

DE89 008378

February 1986

rt

*Work supported by the U. S. Department of Energy, BES-Materials Sciences, under contract W-31-109-ENG-38.

Study of a Model Fermi Liquid Interacting via a Hard-core Repulsive Potential and an Attractive Tail

Tai Kai Ng

Department of Physics and Astronomy
Northwestern University
Evanston, IL 60201

and

K.S. Singwi

Department of Physics and Astronomy
Northwestern University

and

Division of Materials Science and Technology
Argonne National Laboratory
Argonne, IL 60439

ABSTRACT

In this paper we present an extensive microscopic study of the collective and single-particle properties of a model Fermi liquid whose particles interact via a repulsive hard-core potential and an attractive tail. The model system is intended to simulate liquid ^{3}He. The study is based on an approximate scheme of Singwi, Tosi, Land and Sjölander (STLS) which was devised to treat correlations in Coulomb Fermi liquids. The primary aim of this study is to learn whether the model system is capable of reproducing some of the salient features observed in normal liquid ^{3}He, and about the role of the repulsive and attractive parts of the potential. We have calculated the Landau parameters F_0^s and F_0^a and their variation with pressure, the wave number and pressure dependence of the spin-symmetric and spin-antisymmetric polarization potentials, pressure dependence of the dispersion of the zero sound, the static structure factors and the quasiparticle mass. Although we make no quantitative claims when

comparing our calculations with experiments in real liquid ^{3}He, we do conclude that our model system within the frame work of the STLS scheme can account qualitatively for the latter. Besides, since the theory is microscopic in nature and is parameter free, it has enabled us to understand better the role of the repulsive and the attractive parts of the bare potential in determining the properties of liquid ^{3}He.

PACS numbers: 61.20.Ne, 67.50.Dg

I. Introduction:

A low density Fermi gas whose particles interact via a repulsive hard-core potential has been a subject[1,2] of considerable interest over the years, since it forms the basis for studies of nuclear matter and liquid ^{3}He. In this model the physical quantities of interest such as the ground-state energy are expanded in terms of a small parameter $c = k_F a_0$, a_0 being the hard-core radius and $\hbar k_F$ the Fermi momentum. Unfortunately, in real liquid ^{3}He no such small parameter exists, and, therefore, any perturbation approach is doomed to failure from the start. On the otherhand, there are no exact mathematical schemes to treat a dense Fermi liquid. Recourse, has, therefore, to be taken to approximate schemes even to treat simple model systems.

During recent years, numerical techniques of the correlated-basis-function approach[3] have yielded promising results as far as ground-state properties are concerned. Green's function Monte-Carlo method[4] to treat Fermi systems has just begun to be used, although there are some problems. These schemes involve heavy numerical work, and the role of dynamic correlations is not at all clear. The underlying physics is somewhat relegated to the background. Of the several phenomenological theories[5] of liquid ^{3}He, perhaps the most ambitious and successful one is the polarization-potential approach of Aldrich and Pines.[6] Notwithstanding the fact that the latter involves some parameters which need to be adjusted by appealing to experiment, it has some very attractive features. What is now needed is a microscopic understanding of these potentials, which we have attempted to provide in this paper.

The purpose of this paper is to present (i) a detailed microscopic study of the collective and single particle properties of a model Fermi liquid whose particles interact via a repulsive hard- core potential; and (ii) the effect of an attractive tail on these properties. This model system has the virtue that it incorporates two most essential physical features of real liquid ^{3}He: (i) the fermion nature of the atoms and (ii) the hard-core repulsion between the atoms. The approximate scheme that we use to study this model system is the one proposed some years ago by Singwi, Tosi, Land and Sjölander[7] (STLS) to study correlations in electron liquids. This scheme has been tested and found to give very good results for many of the properties of the electron[8] and the electron-hole[9] liquids. It has, hitherto, not been applied to the study of a Fermi liquid interacting via a hard-core potential. Since the model possesses only some resemblance to liquid ^{3}He and since the STLS scheme is only an approximate one, we make no quantitative claims when comparing theory with experiment. We are only striving to know whether the model is capable of reproducing some of the very salient features observed in normal liquid ^{3}He. For example, one would like to know what are the predictions of the model for the magnitude of the two most important Landau parameters F_0^s and F_0^a and their variation with pressure. What is the wave number and pressure dependence of the spin-symmetric and spin-antisymmetric polarization potentials? What is the nature of the dispersion of the zero sound and how does it vary with pressure? How do the density- and spin-fluctuation static structure factors $S(k)$ and $\tilde{S}(k)$ look like and how do they vary with pressure? How does the quasiparticle mass vary with pressure and particle momentum? What is the effect of adding an

attractive tail to the hard- core potential on the above mentioned properties? Questions like these have been studied in this paper within the frame work of the STLS scheme. The answers we obtain seem in general to be consistent with experiment. Besides, since the theory is nonperturbative, it should be possible to compare in the low density limit ($c \ll 1$) its results with the exact results based on the perturbation theory for a hard-core Fermi liquid. The present theory, albeit approximate, is selfconsistent and parameter free. The only input is the bare potential.

II. Theoretical Considerations:

In the STLS scheme[8], the density and spin response function are written in the form of a generalized Random-Phase-Approximation (RPA):

$$\chi_d(k,\omega) = \frac{\chi_0(k,\omega)}{1 - V^s_{eff}(k)\ \chi_0(k,\omega)} \tag{1a}$$

and

$$\chi_s(k,\omega) = - \frac{\mu_B^2\ \chi_0(k,\omega)}{1 - V^a_{eff}(k)\ \chi_0(k,\omega)} , \tag{1b}$$

where χ_d and χ_s are, respectively, the density and spin response functions and χ_0 is the usual Lindhard function. V^s_{eff} and V^a_{eff} are, respectively, the effective spin-symmetric and spin-antisymmetric particle-hole interactions. μ_B is the Bohr magneton. The crucial point in the STLS scheme is that the latter are related to the pair-distribution functions through

$$V^s_{eff}(r) = - \int_r^\infty g(r)\ \frac{dV(r)}{dr}\ dr \tag{2a}$$

and

$$V^a_{eff}(r) = - \int_r^\infty \tilde{g}(r)\ \frac{dV(r)}{dr}\ dr , \tag{2b}$$

where $g(r) = g_{\uparrow\uparrow}(r) + g_{\uparrow\downarrow}(r)$ is the ordinary pair-distribution function, and $\tilde{g}(r) = g_{\uparrow\uparrow}(r) - g_{\uparrow\downarrow}(r)$. $V(r)$ is the bare potential. Notice that the effective interaction in the STLS scheme is static. It is not a parameter of the theory, but arises as a result of an ansatz made on the two-particle Wigner distribution function in the equation of motion for one-particle Wigner distribution function, in order to truncate the heirarchy of equations.[8]

In the present case, we consider a bare potential of the form:

$$V(r) = V_0 \qquad r \le a_0$$
$$= 0 \quad , \qquad r > a_0 \quad , \tag{3}$$

where a_0 is the radius of the hard core and V_0 is a positive number. Clearly, for a hard-core potential $V_0 \to \infty$. Using (3) in (2), we have

$$V^s_{eff}(r) = V_0\, g(a_0) \qquad r \le a_0$$
$$= 0 \qquad r > a_0 \tag{4a}$$

and

$$V^a_{eff}(r) = V_0\, \tilde{g}(a_0) \qquad r \le a_0$$
$$= 0 \qquad r > a_0 \tag{4b}$$

Notice that V^s_{eff} and V^a_{eff} differ only by a constant factor. The Fourier transform of $V^s_{eff}(r)$ is

$$V^s_{eff}(k) = \int d^3r\, e^{i\vec{k}\cdot\vec{r}}\, V^s_{eff}(r)$$

$$= \frac{4\pi V_0 g(a_0)}{k^3} \left[\sin(ka_0) - (ka_0)\cos(ka_0) \right] , \tag{5}$$

and a similar expression is obtained for $V^a_{eff}(k)$ with $g(a_0)$ replaced by $\tilde{g}(a_0)$.

The numbers $g(a_0)$ and $\tilde{g}(a_0)$ are obtained by using the fluctuation-dissipation theorem according to which

$$S(k) = -\frac{3\pi}{k_F^3} \int_0^\infty d\omega\, \mathrm{Im}\, \chi_d(k,\omega) \tag{6a}$$

and

$$\tilde{S}(k) = -\frac{3\pi}{k_F^3} \int_0^\infty d\omega\, \mathrm{Im}\, \chi_s(k,\omega) \quad . \tag{6b}$$

Now

$$g(r) = 1 + \frac{3}{2k_F^3 r} \int_0^\infty kdk \sin(kr) \left[S(k)-1\right] \quad , \tag{7a}$$

and

$$\tilde{g}(r) = \frac{3}{2k_F^3 r} \int_0^\infty kdk \sin(kr) \left[\tilde{S}(k)-1\right] \tag{7b}$$

With $r = a_0$, equations (1), (5), (6) and (7) constitute a set of equations for the numbers $g(a_0)$ and $\tilde{g}(a_0)$, which have to be solved selfconsistently. Let us first consider the equation for $g(a_0)$. Writing, $x = V_0\, g(a_0)$, equations (1a), (5), (6a) and (7a) can be written in the form

$$x/V_0 = F(x) \quad , \tag{8a}$$

where

$$F(x) = 1 + \frac{3}{2k_F^3 a_0} \int_0^\infty kdk \sin(ka_0) \left[S(k;x)-1\right] \quad . \tag{8b}$$

$$S(k;x) = -\frac{3\pi}{k_F^3} \int_0^\infty \mathrm{Im}\, \chi_d(k,\omega;x)\, d\omega \tag{8c}$$

$$\chi_d(k,\omega;x) = \frac{\chi_0(k,\omega)}{1 - V_{eff}(k;x)\chi_0(k,\omega)} \tag{8d}$$

and

$$V_{eff}(k;x) = \frac{4\pi x}{k^3} \left[\sin(ka_0) - ka_0 \cos(ka_0)\right] \tag{8e}$$

Equation (8a) is a nonlinear equation which can be solved without much difficulty. It is worth pointing out here that an iterative procedure to solve (8a) will diverge for large enough V_0 although a solution of the equation exists. This point is discussed in detail in Appendix A. In the limit $V_0 \to \infty$ (hard-core limit), we expect $g(a_0) \to 0$ and the effective interaction $V_{eff}^s(k)$ is determined completely by the

equation $F(x) = 0$. A similar equation can be set up for the case of the spin response. Writing $y = V_0\tilde{g}(a_0)$, the spin-antisymmetric effective interaction is obtained by solving an equation of the form

$$\frac{y}{V_0} = G(y) \quad , \tag{9a}$$

where it can be seen easily that

$$G(y) = F(y)-1 \tag{9b}$$

We have solved equation (8a) and (9b) in the limit $V_0 \to \infty$ numerically using Newton's method for various densities. We find that solutions exist only at densities below a certain critical value. In the density-response case, the critical density is given approximately by $a_0k_F \simeq 2{\cdot}0$; and in the spin case by $a_0k_F \simeq 2{\cdot}6$. Values of $x = V_0g(a_0)$ and $y = V_0\tilde{g}(a_0)$ are given in Table 1 for various values of $c = a_0k_F$.

The absence of a solution beyond a certain critical value of the density suggests that something drastic may be happening in the vicinity of the critical density. In fact, an earlier study of a Bose liquid interacting via a hard-core potential by Hansen etal[10] suggests that the system may solidify at roughly the density $a_0k_F \simeq 1{\cdot}9$.

The Landau parameters $F_0^s = N(0)\ V_{eff}^s\ (k=0)$ and $F_0^a = N(0)\ V_{eff}^a\ (k=0)$, where $N(0)$ is the density of states are shown in Figs. (1a) and (1b) as a function of density. We have expressed the density in terms of a fixed density n_0 given by $n_0^{-1} = \frac{4\pi}{3} a_0^3$. Notice that n_0 is just a mathematically convenient quantity which has no particular physical meaning. It is clear from a comparison of Figs. (1a) and (1b) that F_0^s changes much more rapidly with density as compared to F_0^a in the

region of high density, $c>1$. In fact in the density region $0{\cdot}3 \leq n/n_0 \leq 0{\cdot}7$, F_0^s changes by almost a factor of 10; whereas F_0^a changes by only 30%. This result is in general agreement with what is observed in liquid ^{3}He under pressure. Absolute values of F_0^s and F_0^a of the model do not compare well with those observed in ^{3}He. Moreover, we find that F_0^a becomes less than -1 at $c \approx 1{\cdot}74$, so that the model predicts a ferromagnetic transition at this density. Such a transition is not observed in liquid ^{3}He. At this stage, it is not clear whether the ferromagnetic instability we observe is an artifact of the model itself or an actual artifact of the theory we use.

II. Dilute Hard-core Fermi gas (c<1)

This is the region of density where perturbation theory is valid
ıd has been extensively studied. The perturbation theory results for
<1 can be considered almost exact, and this makes it possible to
›mpare some of our results with the previously known results. The
ılculated Landau parameters F_0^s and $-F_0^a$ are shown in Fig. 2b as a
ınction of c(c≤1). Notice that $-F_0^a \to F_0^s$ as c→0. This result is a
›nsequence of the fact that as c→0, the interaction becomes
ssentially point like thus rendering the Pauli exclusion principle
ry effective. The compressibility ratio K/K_f in our theory is given

$$\frac{K}{K_f} = \frac{1}{1 + F_0^s} \quad , \tag{10}$$

nce m*/m = 1. This ratio is shown in Fig. (2a) (curve 1 as a
ınction of c and compared with the corresponding ratio obtained from
e exact small c expansion of the ground-state energy (curve 2)).[11,12]
e agreement between our result and the exact result is only fair, a
sult which is not totally unexpected, since similar quality of
reement is also obtained in the case of an electron liquid.[8] In a
ter refinement of the STLS theory, Vashishta and Singwi[13] were able
get a very good agreement with the exact result in the electron gas
se. We have not attempted here at present such a refinement of the
eory.

The static structure factor S(k) is shown in Fig. 3 for values of
= 0·4 and 0·6. It is quite structureless at these low densities.
spin-structure factor $\tilde{S}(k)$ is shown in Fig. 4 for the same two
ues of the density. Notice the shift of the peak position of $\tilde{S}(k)$
h increasing density. The corresponding pair correlation functions

$g(r)$ and $\tilde{g}(r)$ are shown in Figs. (5) and (6). Notice that $g(r)$ is nonzero inside the hard-core, although $g(a_0) = 0$. This unphysical feature is found throughout the whole range of density we have studied and should be considered as the defect of the theory. This is a manifestation of the bad behaviour of $S(k)$ for large values of k. This bad behaviour may be slight and may even be not perceptible in a plot of $S(k)$, but it can lead to unphysical behaviour of $g(r)$ for small value of r. The same is true for $\tilde{g}(r)$.

The effective mass m^*/m on the Fermi surface is calculated as a function of density by calculating the selfenergy. The latter is calculated by using an approximate formula derived[14] by us earlier. A brief summary of the underlying theory is given in Appendix B. An exact result[1] for m^*/m based on small c expansion is given below:

$$m^*/m = 1 + \frac{8}{15\pi^2}(7 \log 2 - 1)c^2 + O(c^3) \qquad (13)$$

In Fig. 7 our calculated values of m^*/m as a function of c are compared with those given by eqn. (13). The agreement is quite good in the small c region where eqn. (13) is valid.

IV. High density Hard-Core Fermi liquid (c>1)

The high density region c>1 is of considerable interest, since liquid ^{3}He in a first approximation can be considered as a Fermi liquid interacting via a hard-core potential. Taking $a_0 \simeq 2{\cdot}56$ Å and $k_F \sim 0{\cdot}78$ Å^{-1}, corresponding to the normal liquid ^{3}He density, one finds that c~2. Notice, however, that real liquid ^{3}He interacts via a softer potential with an attractive tail (6-12 L-J potential); and, therefore, the effective c for liquid ^{3}He should be smaller than 2. We shall see in what follows that an appropriate value of c for liquid ^{3}He is c~1·5-1·7.

(i) Zero-Sound Dispersion:

The dispersion of the collective mode of the density fluctuation is obtained in our model by solving the equation:

$$1 - V^s_{eff}(k)\, \chi_0(k,\omega) = 0 \qquad (14)$$

A sharp collective mode exists only for a density greater than a certain critical density when it lies outside the particle-hole continuum. In the present model this critical density is c~0·9. The calculated dispersion for the collective mode for several different values of the density is shown in Fig. 8. There is a remarkable similarity, although qualitative, between the dispersion curve for c~1·7 and the one observed by Skold et al.[15] from inelastic neutron scattering experiments. What is more interesting is the dependence of the dispersion curves on the density of the liquid or the pressure. With the increase in density, there is the flattening of the dispersion curve. Such a flattening has been observed experimentally[15] and was indeed predicted by Pines et al.[16] on the basis

of their phenomenological theory. When the density is high enough, a peak in the dispersion curve builds up at around $ka_0 \sim 3$. A similar prediction has also been made by Glyde and Khanna[17] based on their phenomenological theory. The question what happens to the dispersion curve when a small attractive potential is added to the hard-core will be examined in Section VI.

(ii) The Static-Structure Factors:

The static structure factor S(k) for three different densities is shown in Fig. 9. As expected, the peak in the structure factor increases in height with the increase in density, but the position of the peak remains unchanged at around $ka_0 \simeq 5.0$. Notice also that a small plateau that is observed[18,19] in S(k) at small $k \sim 0{\cdot}3\text{Å}^{-1}$ in liquid ^{3}He is absent here. A more detailed discussion on this point will be given in Section VI, where the effect of adding an attractive part to the hard-core potential will be discussed. The pair-correlation functions g(r) obtained by Fourier transforming the S(k)'s of Fig. 9 for two different densities are shown in Fig. 10. For $r<a_0$, the unphysical nature of g(r) is obvious. When the density becomes high, the oscillations in g(r) persist for large values of r/a_0.

The magnetic structure factor $\tilde{S}(k)$ is shown in Fig. 11 for two different densities. The appearance of a sharp spike in $\tilde{S}(k)$ for $c=2{\cdot}0$ is an indication that the normal state is no longer the stable state in the present model. In fact for $c=2{\cdot}0$, $F_0^a < -1$, so that the system should be already ferromagnetic. In contrast to the behaviour of S(k), we find that the overall shape of $\tilde{S}(k)$ in the normal state is quite insensitive to the density change except that the position of the tiny peak in $\tilde{S}(k)$ shifts towards larger values of k as the density

increases. The corresponding pair-correlation function $\tilde{g}(r)$ is shown in Fig. 12. Notice that despite the unphysical nature of $\tilde{g}(r)$ for $r<a_0$, it is less than zero for all values of $r>a_0$ - a result which is in agreement with the conclusion drawn from a simple argument based on Pauli principle.

(iii)Effective Mass

The effective mass on the Fermi surface is defined by

$$\frac{m^*}{m} = \left. \frac{1 - \frac{\partial}{\partial \omega} \text{ Re } \Sigma(k,\omega)}{1 + \frac{\partial}{\partial \varepsilon_k} \text{ Re } \Sigma(k,\omega)} \right|_{\substack{k=k_F \\ \omega=0}} \tag{15}$$

Figure (13) shows the results of our effective mass calculation on the Fermi surface over a range of densities when $F_0^a > -1$ ie the normal state is the stable paramagnetic state. Notice that a rather large mass renormalization coming from spin fluctuations is found over the entire density range. A divergence in the effective mass is found for $c \simeq 1 \cdot 74$ which is the result of the paramagnon effect.

We have also calculated the quasiparticle spectrum in the "on-shell" approximation.

$$E_p = \varepsilon_p + \text{Re } \Sigma(p, \varepsilon_p) \quad , \tag{16}$$

where ε_p is measured from the Fermi energy and Re Σ is the real part of the selfenergy. The results for two different densities are shown in Fig. 14. These curves for quasiparticle spectrum exhibit qualitative similarity to the corresponding curve calculated by Padharipande et al.[20] The momentum dependent effective mass

$$\left[\frac{m^*}{m}(p) \right]^{-1} = \frac{\partial E_p}{\partial \varepsilon_p} \tag{17}$$

is shown in Fig. 15 for the same two values of density. The shape of

these curves is similar to the shape calculated by Friman and Krotscheck.[21] The second peak around $k/k_F = 1{\cdot}65$ is due to the zero-sound contribution. Notice that the "on-shell" value $\simeq 7{\cdot}3$ of $m^*(k)/_m$ on the Fermi surface is much larger than the corresponding value of $1{\cdot}22$ as read from curve 1 of Fig. 13. The latter is based on the definition of the effective mass as given by formula (15). This large difference is an artifact of the "on-shell" approximation, which cannot be trusted when $\frac{\partial}{\partial\omega}$ Re $\sum(k,\omega)$ is large and negative.

V. Effect of an Attractive Tail:

In real liquid ^{3}He, the interatomic potential is not a hard-core potential but a potential of the Lennard-Jones kind with an attractive tail. The latter plays an important role in determining the properties of liquid ^{3}He. In fact the stability of the system depends entirely on the existence of such a tail. Hitherto, in the absence of any microscopic theory of liquid ^{3}He, it has not been possible to say even qualitatively what is the effect of the attractive tail of the potential on physical quantities such as the structure factors $S(k)$ and $\tilde{S}(k)$, the zero-sound dispersion and the Landau parameters F_0^s and F_0^a. In this section we shall examine the effect of such an attractive tail with an approximated model. We shall see that some very interesting results emerge.

For simplicity, we consider a model interaction which can be solved easily:

$$\begin{aligned} V(r) &= V_0 && r<a_0 \\ &= -\varepsilon && a_0<r<a_1 \\ &= 0 && a_1<r \end{aligned} \tag{18}$$

The parameters a_1 and ε of the attractive tail are fixed by requiring that

$$\int_\sigma^\infty V_{L-J}(r)\, r^2 dr = \int_{a_0}^{a_1} (-\varepsilon)\, r^2 dr \tag{19a}$$

and

$$\int_\sigma^\infty r\, V_{L-J}(r)\, r^2 dr = \int_{a_0}^{a_1} r(-\varepsilon)\, r^2 dr \tag{19b}$$

where V_{L-J} is the Lennard-Jones potential for ^{3}He

$$V_{L\text{-}J}(r) = 4\,\varepsilon\left[\left(\frac{\sigma}{r}\right)^{12} - \left(\frac{\sigma}{r}\right)^{6}\right]$$

Furthermore, we take $a_0 \simeq 0{\cdot}9\sigma$ to account roughly for the fact that L-J potential has a weaker repulsive core compared with the hard-core potential. With the requirements (19), we find that

$$\left.\begin{aligned} a_1 &\simeq 2{\cdot}05\; a_0 \\ \varepsilon &\simeq 0{\cdot}46\;\tilde{\varepsilon} \end{aligned}\right\} \tag{20}$$

From eqns. (2) and (18), it follows that

$$V^{s}_{eff}(r) = \begin{cases} 0 & r>a_1 \\ -\,\varepsilon\, g(a_1) & a_1>r>a_0 \\ -\,\varepsilon\, g(a_1) + (V_0+\varepsilon)g(a_0) & r<a_0 \end{cases} \tag{21a}$$

and

$$V^{a}_{eff}(r) = \begin{cases} 0 & r>a_1 \\ -\,\varepsilon\tilde{g}(a_1) & a_1>r>a_0 \\ -\,\varepsilon\tilde{g}(a_1)+(V_0+\varepsilon)\tilde{g}(a_0) & r<a_0 \end{cases} \tag{21b}$$

The Fourier transform of the effective potential $V^{s}_{eff}(r)$ is

$$V^{s}_{eff}(k) = \frac{4\pi}{k^3}(V_0+\varepsilon)g(a_0)\left[\sin(ka_0) - ka_0\cos(ka_0)\right]$$

$$- \frac{4\pi}{k^3}\,\varepsilon\, g(a_1)\left[\sin(ka_1) - ka_1\cos(ka_1)\right] \quad , \tag{22}$$

and a similar expression for $V^{a}_{eff}(k)$ with $g(r)$ replaced by $\tilde{g}(r)$.

As in section II, a set of selfconsistent equations for the variables $x_1 = (V_0+\varepsilon)g(a_0)$, $x_2 = -\,\varepsilon\, g(a_1)$ and $y_1 = (a_0+\varepsilon)\tilde{g}(a_0)$ and $y_2 = -\,\varepsilon\,\tilde{g}(a_1)$ can be set up. However, the computation is some what more involved here because one has now to solve two coupled nonlinear

equations of two variables. Proceeding as before, we can write these equations in the form:

$$\frac{x_1}{(V_0+\epsilon)} = F_1(x_1,x_2) \tag{23a}$$

$$\frac{x_2}{\epsilon} = F_2(x_1,x_2) \ , \tag{23b}$$

where

$$\left.\begin{aligned} F_1(x_1,x_2) &= g(a_0;x_1,x_2) \\ F_2(x_1,x_2) &= g(a_1;x_1,x_2) \end{aligned}\right\} \tag{24}$$

and

$$\frac{y_1}{(V_0+\epsilon)} = G_1(y_1,y_2) \tag{25a}$$

$$\frac{y_2}{\epsilon} = G_2(y_1,y_2) \ , \tag{25b}$$

where

$$\left.\begin{aligned} G_1(y_1,y_2) &= \tilde{g}(a_0;y_1,y_2) \\ G_2(y_1,y_2) &= \tilde{g}(a_1;y_1,y_2) \end{aligned}\right\} \tag{26}$$

In the limit $V_0 \to \infty$, we have as before

$$F_1(x_1,x_2) = 0 \tag{27}$$

and $$F_2(x_1,x_2) - \frac{x_2}{\epsilon} = 0 \ ,$$

and a similar set of equations for the spin response.

VI. Results and Discussion:

We have solved the above set of equations numerically, using the generalized Newton's method, for different densities (c-values), and the results are given in Table II.

(a) Landau parameters:

The resulting Landau parameters F_0^s and F_0^a are shown in Figs. 16 and 17, respectively, where for comparison sake hard-core potential values are also shown. There are several interesting features to note. The attractive part has the effect of reducing F_0^s and increasing F_0^a compared to their values in the pure hard-core case. Also the curve for F_0^s in the region of low density is much steeper than it is for the hard-core. In fact, it clearly shows the tendency of becoming negative for $c<1\cdot3$. It is, therefore, no surprise that for nuclear matter where $c<1$, F_0^s is negative. The effect of an attractive tail on F_0^a is very large as can be seen in Fig. 17 so much so that in the region of densities where hard-core $F_0^a<-1$ (ie ferromagnetic), the inclusion of an attractive tail has resulted in $F_0^a>-1$. Under the circumstances, it is natural to ask whether our results are sensitively dependent on the shape of the attractive part of the bare potential. To answer this question, we have solved the selfconsistent equations also for two other choices of the parameters ϵ and a_1 for $c=1\cdot6$. The latter satisfy the requirement imposed by eqn.(19a). The resulting effective interactions $V^s_{eff}(k)$ and $V^a_{eff}(k)$ for three different choices of the parameters a_1 and ϵ are shown in Fig. 18 and Fig. 19, respectively. Notice that $V^s_{eff}(k)$ is qualitatively quite stable against variation of a_1 except in the small k-region, where the Landau parameter F_0^s $\left[V^s_{eff}(k=0)N(0)\right]$ for three

different situations does not differ by more than 20%. The situation is entirely different for $V^a_{eff}(k)$ as can be seen in Fig. 19. The value of F^a_0 $\left[V^a_{eff}(k=0)N(0)\right]$ depends very sensitively on the shape of the potential. In fact F^a_0 changes from 0·27 to -0·44 for three different shapes of the attractive potential chosen. The main reason for this being the change in the values of $\tilde{g}(a_1)$ for different values of a_1; the latter being always close to zero and as such can differ easily by one hundred precent although the actual numerical difference may be small. As a result, we conclude that the spin-antisymmetric effective interaction depends very sensitively on the shape of the bare potential. In particular, our results for F^a_0 can not be trusted as reasonable approximations for liquid ^{3}He. On the contrary, our results for the symmetric case can be considered as reasonable first approximations for liquid ^{3}He. Notwithstanding that, our $N(0)V^a_{eff}(k)$ for $a_1 \simeq 2\cdot 2a_0$ (see Fig. 19) is qualitatively very similar to the corresponding polarization potential of Aldrich and Pines (^{3}He at SVP).

In Fig. 20, we have compared $N(0)\ V^a_{eff}(k)$ in the two cases one with a pure-hard core potential and the other a hard-core plus an attractive potential for a given density $c=1\cdot 7$. Notice that in the small k region, inclusion of an attractive tail in the potential brings about a drastic change in the shape of the effective potential. F^a_0 increases by more than a factor of 2 from its hard-core value thus shifting the magnetic instability to higher densities. Curve B of Fig. 20 has indeed a shape very much like that of $f^a(k)$ of Aldrich and Pines.[6] The minimum in the effective potential is around $k \simeq 0\cdot 8\text{Å}^{-1}$ and depends on the shape of the attractive part of the potential.

The spin-symmetric effective interactions $V^s_{eff}(k)N(0)$ for c=1·5 and c=1·9 are plotted in Fig. 21 and Fig. 22, respectively. The corresponding effective interaction for the pure hard-core potential is also shown for comparison. Notice that $N(0)V^s_{eff}(k)$ for c=1·5 is qualitatively quite similar to the polarization potential $f^s(k)$ of Aldrich and Pines.[6] It starts with a value 10 and has a maximum around $ka_0 \simeq 1·5$ $(k/k_F \simeq 1)$. This maximum is not so pronounced as in the $f^s(k)$ of Aldrich and Pines. It first attains a value zero around $ka_0 \simeq 4·5$ $(k/k_F \simeq 3)$, whereas $f^s(k)$ does so at $k/k_F \simeq 2·2$. This difference could easily arise from the difference in the hard-core part of the potential. Notice (Fig. 21) that the inclusion of an attractive tail brings about a considerable reduction in the value of $N(0)V^s_{eff}(k)$ for small values of k from its hard-core value and a change in the shape. Actually, it can be shown easily by expanding (22) for small values of k that the dip in $N(0)V^s_{eff}(k)$ is the result of the attractive part of the potential and is present only when the ratio $r = \varepsilon g(a_1)/(V_0+\varepsilon)g(a_0)$ exceeds a certain critical value. Similar structure is not present in $N(0)V^s_{eff}(k)$ (Fig. 22) for c=1·9. In fact it can be seen from Table II that the ratio r decreases as the density increases resulting in a gradual disappearance of the structure. This is understandable since at high densities one expects the effect of the hard-core to be the dominating one.

(b). <u>The Structure Factors</u>:

The selfconsistent static structure factors S(k) for three different densities are shown in Fig. 23. The peak height increases with density as expected, whereas the peak position remains unaffected. At a first glance, the curves of Fig. 23 appear to be the

same as those of Fig. 9 for a pure hard-core potential. However, on closer examination an interesting difference is discerned when one compares the inserts of Figs. (9) and (23), where S(k) for small values of ka_0 is shown on an expanded scale. Notice that for c=1·5, S(k) for the hard-core (Fig. 9) is convex to the wave number axis; whereas the S(k) of Fig. 23 for a hard-core plus an attractive potential is concave, leading to a plateau-like structure in S(k). Such a structure has indeed been seen experimentally in S(k) of liquid ^{3}He through x-ray and neutron scattering experiments.[18,19] Putting a_0=2·5Å, we see that the position of the plateau is also in rough agreement with what is observed. The occurrence of this plateau can be traced to the structure in the low k region of $N(0)V^s_{eff}(k)$ for c=1·5. This structure disappears with increasing density. Based on this observation, we conclude that the observed plateau-like structure in S(k) in the small k region in liquid ^{3}He is a result of an attractive part of the potential between the helium atoms; and that the structure would weaken and ultimately vanish as the density of the system increases when the repulsive part of the potential dominates. Since this effect is quite independent of statistics, a similar behaviour is also expected to be found in the structure factor of liquid ^{4}He.

The pair-correlation functions g(r) for c=1·5 and 1·7 are shown in Fig. 24. These curves are very similar to the corresponding ones for the pure hard-core potential Fig. 10. The difference is almost negligible over the entire range of r. The behaviour of g(r) for $r<a_0$ is obviously, unphysical. As expected, with the increase in density the oscillations in g(r) become more pronounced.

The structure factors $\tilde{S}(k)$ for spin fluctuations for three different densities are shown in Fig. 25. The shape of these curves is quite different from that in the pure hard-core case, Fig. 11. This difference is a consequence of the very different behaviour of $V^a_{eff}(k)$ in the region of a small $\underline{k}$ in the two cases. As the density increases, the effect of the hard core becomes more dominant and the peak in $\tilde{S}(k)$ weakens and ultimately disappears. We expect, at least qualitatively, a similar behaviour in liquid ^{3}He.

In Fig. 26, we have shown $\tilde{g}(r)$ for two different densities. Although the general shape of these curves is very similar to the shape of the corresponding curves in the hard-core case, Fig. 10, the magnitude of $\tilde{g}(r)$ is different.

(c). Zero-Sound Dispersion:

The zero-sound dispersion for four different densities is shown in Fig. 27. On comparing these curves with the corresponding curves in Fig. 8 for the pure hard-core case, one notices two important differences: (i) The velocity of the zero-sound mode given by the slope of these curves for $ka_0 \to 0$, is reduced from its hard-core value, since F_0^s is reduced. (ii) A more pronounced flattening of the dispersion curves in the large k-region is seen for say c=1·7 compared to that seen in Fig. 8. Also for higher densities (c>1·7), the peak in the dispersion curves is more pronounced than what it is in Fig. 8. It seems that the addition of an attractive part to the bare hard-core inter-particle potential does bring the zero-sound dispersion more in agreement with experiment in liquid ^{3}He (c~1·7-1·6), although the present agreement remains qualitative. For c=1·7, the flattening is around $ka_0 \simeq 3 \cdot 2$ i.e. $k \simeq 1 \cdot 2 \text{Å}^{-1}$.

II. Concluding Remarks:

In the introduction we asked ourselves a number of questions the ain thrust of which was whether it is possible to understand from icroscopic considerations, at least qualitatively, some of the triking features seen experimentally in the properties of normal iquid ^{3}He. Using a model of the Fermi liquid, whose particles nteract via a repulsive hard-core and an attractive tail, we have alculated a number of properties of our model system within the frame ork of the STLS theory and have provided an answer in the affirmative. ince the theory is microscopic, it has enabled us to study separately he effect of the pure hard-core and attractive parts of the potential hich has, hitherto, not been possible. Our calculations have provided ome support to the form of the phenomenological polarization otentials of Aldrich and Pines in liquid ^{3}He. Remarkably enough, it rns out that the theory also has some predictive power. For ample, it predicts the flattening of the dispersion curve of the zero- ound and the development of a peak in it with increasing density. It lso predicts, unexpectedly, one very subtle feature that of the currence of a plateau in the static structure factor S(k) in the gion of small wave number and its gradual disappearance with ncreasing density. It appears that this is a common property of both quid ^{3}He and ^{4}He, and is a consequence of the attractive tail of the tential. Above all, the present study has provided us with some ysical insight into the nature of normal liquid ^{3}He. A comparison of r results with the exact results for a low density ($c \ll 1$) hard-core rmi liquid shows that the agreement between the two is a niquantitative one.

We would now like to make some comments on the course of future work. An obvious question which comes to ones mind is what changes would ensue if one were to repeat the present calculation using a more realistic Lennard-Jones kind of potential. In principle there is no difficulty in doing so, but in practice one is faced with a gigantic numerical task of solving selfconsistently a nonlinear integral equation. For a soft coulomb potential, a straight forward iteration procedure has been used successfully, but for a Lennard Jones potential this does not seem to work. And so far we have been unable to find a fast converging numerical procedure. We, however, believe that it is purely a technical matter since in this paper we have been able to demonstrate that the theory gives a convergent answer even for a hard-core potential. In Appendix A we have explicitly shown that a straight forward iteration procedure under certain conditions fails to find a solution even though the latter exists.

A more difficult and fundamental problem which still remains with the STLS approximation is of incorporating in a consistent manner frequency and wavenumber dependent selfenergy effects such that in the static long wave length limit one arrives at the Landau form for the compressibility and susceptibility expressions. So far we have used the effective dynamic interaction to calculate the effective mass of the quasiparticle - a procedure analogous to that of Ref. 21.

Extension of the present calculation to polarized Fermi systems is interesting and is at present under investigation.

ACKNOWLEDGMENTS

This work was supported in part by the Material Research Center of Northwestern University under NSF grant No. DMR-79-23573 and in part by the Department of Energy.

Table I Solution of the STLS equation for various densities for a pure hard-core potential

$C\ (a_0 k_F)$	n/n_0	$V_0 g(a_0)$	$-V_0 \tilde{g}(a_0)$
0.1		159.31	157.88
0.2		42.98	41.56
0.3		20.94	19.44
0.4		13.12	11.50
0.5		9.51	7.73
0.6		7.62	5.64
0.7		6.59	4.34
0.8		6.06	3.48
0.9		5.91	2.87
1.0		6.10	2.42
1.1		6.69	2.07
1.2		7.86	1.80
1.3		10.14	1.57
1.4	0.39	15.31	1.38
1.5	0.48	26.55	1.22
1.6	0.58	37.27	1.07
1.7	0.69	38.96	0.94
1.8	0.82	36.45	0.82
1.9	0.97	31.81	0.72
2.0	1.13	26.88	0.64

Table II Solution of the STLS equation for various densities for a hard-core plus a rectangular attractive potential

$C\ (a_0 k_F)$	$V_0 g(a_0)$	$\varepsilon g(a_1)$	$-V_0 \tilde{g}(a_0)$	$-\varepsilon \tilde{g}(a_1)$
1.4	16.19	1.60	2.11	0.305
1.5	24.91	1.32	1.73	0.211
1.6	35.09	1.07	1.44	0.144
1.7	37.63	0.88	1.21	0.095
1.8	35.88	0.73	1.02	0.060
1.9	31.48	0.62	0.85	0.034
2.0	29.40	0.56	-	-

APPENDIX A

Here we make some comments on the solution of the STLS equation for a strong repulsive potential. For an arbitary potential, the STLS equations (1), (2), (6) and (7) can be written as an integral equation for the pair-correlation function g(r) in the form

$$g(r) = F(r,g(r)) \qquad A(1)$$

where F is a functional of g(r). To solve the integral equation, the most common procedure is first to write the integral equation in the form of non-linear matrix equations on discrete sites, (r_i i=1,...,N) so that the continuous limit is recovered as N→∞.

The matrix equation can be written schematically in the form

$$x_i = F_i(x_1,x_2,\ldots,x_N) \qquad i=1,\ldots,N \qquad A(2)$$

where in the case of STLS equation, $x_i = g(r_i)$. This equation is usually solved by iteration where

$$x_i^{(n)} = F_i(x_1^{(n-1)},x_2^{(n-1)},\ldots x_N^{(n-1)}) \qquad i=1,\ldots,N \qquad A(3)$$

until convergence is attained. However, in the STLS equation, it is often found that the iteration procedure diverges for a strong repulsive potential. For a general N-variable equation like A(1), it is very hard to understand the origin of the divergence; whether it is an artifact of the iteration procedure, or whether it is an indication that the equation has actually no solution. However, in our present situation the STLS equation is an equation of one variable (or two in Section V) for which the above questions can be answered unambigiously.

To show this, we examine our STLS equation for a pure hard-core potential (Eq. (8a) of the text)

$$\frac{x}{V_0} = F(x) \qquad A(3)$$

In Fig. (28), we show the function F(x) as a function of x for c = 1·4 and we have also shown the straight line $y = x/V_0$ for two arbitrary values of V_0. The solution of A(3) is given by the intersection of the two curves, $y = F(x)$ and $y = x/V_0$. It is obvious from Fig. (28) that the solution of A(3) exists for all values of positive V_0 for the particular form of F(x) we have.

An iterative solution of A(3) is built up by putting

$$\frac{x_1}{V_0} = F(x_0)$$

$$\frac{x_2}{V_0} = F(x_1)$$

- - - - -
- - - - -

The iterative procedure can be indicated schematically in Fig. (28) by the dashed arrows. Notice that although for both values of V_0 we take, solution undoublty exists; the iterative procedure converges only in the case of a weaker V_0. A more careful analysis shows that the convergence of the iteration procedure depends very strongly on the relative slopes of the two intercepting curves near the intercepting point. Thus we find that although solution for A(3) exists, an iterative procedure is not going to converge when the number $1/V_0$ is too small.

In the simple one-variable (and two variable) case we have considered here, the solution can be attained by other well-developed methods like Newton's Method where convergence is good over the whole range of V_0. In the N variable case, a generalization of Newton's

method exists which relies on the heavy computation of the inverse of a NxN matrix. With modern super computers such a computation becomes possible and calculations should be done to test the theory on a wider range of problems.

APPENDIX B

In a study of single-particle properties in electron-hole liquid, we derived an expression for the one-particle self energy for a multi-component-paramagnetic Fermi liquid. The method is based on an approximate scheme of classification and summation of diagrams introduced by Vignale and Singwi[22]. Here we summarize briefly our results for a one - component paramagnetic Fermi liquid.[14]

An expression for the derivative of self-energy is derived which has the form

$$\delta\Sigma(p) = \int \frac{d^4p'}{(2\pi)^4} \; \psi_{eff}(p,p') \; \delta G^{o}(p'), \qquad B(1)$$

where p,p' are 4 - momenta. $\psi_{eff}(p,p')$ consists of three terms coming from three different physical process: (i) a generalized T-matrix T(p,p') which describes the scattering of two particles, (ii) induced interaction <u>via</u> density fluctations and (iii) induced interaction <u>via</u> spin-fluctations.

In a 'local' approximation

$$\psi_{eff}(p,p') \simeq \psi_{eff}(p-p'), \qquad B(2)$$

We get

$$\psi_{eff}(q) = T(q) + \left[V_{eff}^{s}(q)\right]^2 \chi_s(q) + 3\left[V_{eff}^{a}(q)\right]^2 \chi_a(q) \qquad B(3)$$

where $V_{eff}^{s}(q)$ and $V_{eff}^{a}(q)$ can be identified as our spin-symmetric and spin-antisymmetric interaction introduced in the main text. χ_s and χ_a are the density and spin response functions, respectively. The factor 3 is coming from spin-degeneracy. T(q) should be considered as a 'local' approximated T-matrix. A previous study of Lowy and Brown[23] on electron gas shows that T(q) can be identified roughly as $V_{eff}^{s}(q)$. We have adopted this approximation in our calculation. It

is worth pointing out that $\psi_{eff}(q)$ of eq. (B3) has the same form as the effective interacton which is used by Friman and Krotscheck[21] for a self-energy calculation for liquid ^3He.

Within the local approximation, equation (B-1) can be solved to give

$$\Sigma(p) = \int \frac{d^4q}{(2\pi)^4} \psi_{eff}(q)\, g^{\circ}(p-q) \qquad +\mu^* \qquad \text{B(4)}$$

Notice that the absolute value of self-energy (i.e. the chemical potential) is inacessible using this effective interaction.

The self-energy (B-4) is evaluated by first dividing it into two parts, $\Sigma^{(res)}$ and $\Sigma^{(line)}$[24], where

$$\Sigma^{(Res)}_{(p,\varepsilon)} = \int \frac{d^3q}{(2\pi)^4} \psi_{eff}(q,\ \xi_{\underset{p+q}{\rightarrow}\ \underset{p+q}{\rightarrow}} - \varepsilon) \left[\theta(\varepsilon - \xi_{\underset{p+q}{\rightarrow}\ \underset{p+q}{\rightarrow}}) - \theta(-\xi_{\underset{p+q}{\rightarrow}\ \underset{p+q}{\rightarrow}})\right] \qquad \text{B(5)}$$

and

$$\Sigma^{(line)}_{(p,\varepsilon)} = \frac{m}{2p} \int_0^{\infty} \frac{q\,dq}{(2\pi)^3} \int_{-\infty}^{\infty} d\omega \psi_{eff}(q,i\omega)\ ln \left\{ \frac{\omega^2 + \left[\varepsilon - \xi_{\underset{p+q}{\rightarrow}\ \underset{p+q}{\rightarrow}}\right]^2}{\omega^2 + \left[\varepsilon - \xi_{\underset{p+q}{\rightarrow}\ \underset{p+q}{\rightarrow}}\right]^2} \right\} \qquad \text{B(6)}$$

and $\Sigma = \Sigma^{(Res)} + \Sigma^{(line)}$.

It is easy to show that

$$\frac{\partial \Sigma^{(Res)}_{(p,\varepsilon)}}{\partial \varepsilon} \Bigg|_{\substack{p=1 \\ \varepsilon=0}} = \frac{1}{8\pi^2} \int_0^2 q'dq'\ \psi_{eff}\ (q',0) \qquad \text{B(7a)}$$

$$\frac{\partial \Sigma^{(Res)}_{(p,\varepsilon)}}{\partial \varepsilon_p} \Bigg|_{\substack{p=1 \\ \varepsilon=0}} = 0 \qquad \text{B(7b)}$$

$$\frac{\partial \Sigma^{(line)}_{(p,\varepsilon)}}{\partial \varepsilon} \Bigg|_{\substack{p=1 \\ \varepsilon=0}} = \frac{-1}{8\pi^3} \int_0^{\infty} q\,dq \int_0^{\infty} d\omega\ \psi_{eff}(q,i\omega q) \qquad \text{B(7c)}$$

$$\times \left\{ \frac{2+q}{\omega^2 + (2+q)^2} - \frac{(q-2)}{\omega^2 + (q-2)^2} \right\}$$

$$\left.\frac{\partial\Sigma^{(line)}(p,\varepsilon)}{\partial\varepsilon_p}\right|_{\substack{p=1\\ \varepsilon=0}} = \frac{-1}{32\pi^3}\int_0^\infty q\,dq\int_0^\infty d\omega\;\psi_{eff}(q,i\omega q) \qquad B(7d)$$

$$\times\left\{q\ell n\left[\frac{\omega^2+(2+q)^2}{\omega^2+(q-2)^2}\right]-4\left[\frac{(1+q)(q+2)}{\omega^2+(q+2)^2}-\frac{(1-q)(q-2)}{\omega^2+(q-2)^2}\right]\right\}$$

where we have expressed momentum in units of k_F and ε in units of E_F $p\to p/k_F$ $\varepsilon\to\varepsilon/E_F$. Using the above equation, the effective mass on the fermi surface can be evaluated numerically.

The on-shell effective mass is evaluated by evaluating $\Sigma(p,\xi_p)$ first and then differentiating it numerically with respect to p to get $m^*/m(p)$.

From (B-5), it can be shown after some algebra that for $p>1$

$$\Sigma^{(Res)}(p,\xi_p) = \frac{1}{8\pi^2 p}\int_0^{2p} q\,dq\int_{\max(1-p^2,q^2-2pq)}^{0} dx\;\psi_{eff}(q,x) \qquad B(8a)$$

and for $p<1$

$$\Sigma^{(Res)}(p,\xi_p) = \frac{-1}{8\pi^2 p}\int_0^{2p} q\,dq\int_0^{\min(1-p^2,q^2+2pq)} dx\;\psi_{eff}(q,x)$$

$$-\frac{1}{8\pi^2 p}\int_{2p}^{p+1} q\,dq\int_{q^2-2pq}^{\min(1-p^2,q^2+2pq)} dx\;\psi_{eff}(q,x) \qquad B(8b)$$

Also, from (B-6), we have

$$\Sigma^{(line)}(p,\xi_p) = \frac{1}{16\pi^3 p}\int_0^\infty q^2\,dq\int_0^\infty d\omega\;\psi_{eff}(q,i\omega q)\,\ell n\left|\frac{\omega^2+(2p+q)^2}{\omega^2+(2p-q)^2}\right| \qquad B(9)$$

The above integrals are evaluated numerically.

FIGURE CAPTIONS:

Fig. 1a. Landau parameter F_0^s versus n/n_0 for a hard-core potential.

Fig. 1b. Landau parameter F_0^a versus n/n_0 for a hard-core potential.

Fig. 2a. Ratio K/K_f of the interacting to the free particle compressibility as a function of c. Curve 1 our result; curve 2, exact result.

Fig. 2b. Calculated Landau parameters F_0^s and $-F_0^a$ versus c for small values of c.

Fig. 3. Static structure factor S(k) versus ka_0 for c = 0·4 and 0·6.

Fig. 4. Spin-fluctuation static structure factor $\tilde{S}(k)$ versus ka_0 for c = 0·4 and 0·6.

Fig. 5. Pair-correlation function g(r) versus r/a_0 for c = 0·4 and 0·6.

Fig. 6. Pair-correlation function $\tilde{g}(r)$ versus r/a_0 for c = 0·4 and 0.6.

Fig. 7. Effective mass m*/m on the Fermi surface versus c. Curve 1, exact result of the perturbation theory; and Curve 2, present calculation.

Fig. 8. Dispersion of the zero-sound mode $\omega(k)/E_F(n_0)$ versus ka_0 for four different values of the density.

Fig. 9. Static structure factor S(k) versus ka_0 for densities c = 1·5, 1·7 and 1·9. The insert is the magnified version of S(k) for small values of ka_0.

The dashed line represents the slope of S(k) for $ka_0 \to 0$.

Fig. 10. Pair-correlation function g(r) versus r/a_0 for c = 1·5 and 1·7.

Fig. 11. Structure factor $\tilde{S}(k)$ versus ka_0 for c = 1·6 and 2·0.

Fig. 12. Pair correlation function $\tilde{g}(r)$ versus r/a_0 for c = 1·6 and 2·0.

Fig. 13. Effective mass m^*/m on the Fermi surface versus n/n_0. Curve 1, combined contribution of density and spin fluctuations; Curve 2, contribution of density fluctuations only.

Fig. 14. "On-shell" Quasiparticle energy $E(k)/E_F$ versus k/k_F for c = 1·2 and 1·3. ε_k is the free particle energy measured from the Fermi energy.

Fig. 15. "On-shell" effective mass $\frac{m^*(k)}{m}$ as a function of k/k_F for c = 1·2 and 1·3.

Fig. 16. Landau Parameter F_0^s versus $\frac{n}{n_0}$. Solid curve, hard-core potential only; dashed curve, hard-core + attractive tail.

Fig. 17. Landau Parameter F_0^a versus n/n_0-Solid curve hard-core potential only; dashed curve, hard-core + attractive tail.

Fig. 18. Spin-symmetric dimensionless effective interaction $N(0)V^s_{eff}(k)$ versus ka_0 for c = 1·6 and for three different choices of the parameter a_1 (and ε) for the attractive tail.

Fig. 19. Spin-antisymmetric dimensionless effective interaction $N(0)V^a_{eff}(k)$ versus ka_0 for c = 1·6 and for three different choices of the parameter a_1 (and ε) for the attractive tail.

Fig. 20. Spin-antisymmetric dimensionless effective interaction $N(0)V^{a}_{eff}(k)$ versus ka_0 for $c = 1{\cdot}7$. Curve A is for a pure hard-core potential; and curve B for a hard-core plus an attractive potential.

Fig. 21. Spin-symmetric dimensionless effective interaction $N(0)V^{s}_{eff}(k)$ versus ka_0 for $c = 1{\cdot}5$. Curve A is for a pure hard-core potential and Curve B is for a hard-core plus an attractive potential.

Fig. 22. Spin-symmetric dimensionless effective interaction $N(0)V^{s}_{eff}(k)$ versus ka_0 for $c = 1{\cdot}9$. Curve A is for a pure hard-core potential and Curve B is for a hard-core plus an attractive potential.

Fig. 23. Structure factor S(k) versus ka_0 for $c = 1{\cdot}5$, $1{\cdot}7$ and $1{\cdot}9$. The insert is a magnified version of S(k) for small values of ka_0. The dashed line represents the slope of S(k) for $ka_0 \to 0$.

Fig. 24. Pair-correlation function g(r) versus r/a_0 for $c = 1{\cdot}5$ and $1{\cdot}7$ for a hard-core potential plus an attractive tail.

Fig. 25. Static-structure factor $\tilde{S}(k)$ versus ka_0 for $c = 1{\cdot}5$, $1{\cdot}7$ and $1{\cdot}9$.

Fig. 26. Pair-correlation function $\tilde{g}(r)$ versus r/a_0 for $c = 1{\cdot}5$ and $1{\cdot}7$.

Fig. 27. Zero-sound dispersion $\omega(k)/E_F(n_0)$ versus ka_0 for $c = 1{\cdot}5$, $1{\cdot}7$, $1{\cdot}9$ and $2{\cdot}0$.

Fig. 28. "F(x)" for $c = 1{\cdot}4$. The dashed arrows indicate a straight forward iteration procedure.

REFERENCES

1. A.A. Abrikosov, L.P. Gorkov and I.E. Dzyaloshinsky, Methods of Quantum Field Theory in Statistical Physics (Prentic-Hall, Englewood Cliffs, 1963).

2. A.L. Fetter and J.D. Walecka, Quantum Theory of Many-Particle Systems (McGraw-Hill, New York, 1971).

3. J.W. Clark and E. Krotscheck, Lecture Notes in Physics 198 (Proceedings Odenthal-Altenberg, Germany 1983. Recent Progress in Many-Body Theories) Springer-Verlag 1984, and references therein

4. D.M. Ceperley and M.H. Kalos, Topics in Current Physics 7 (Monte Carlo Methods in Statistical Physics) Springer-Verlag 1979; and references there in.

5. See e.g. K. Levin and O.T. Valls, Physics Reports 98, No. 1 (1983) and references therein.

6. C.H. Aldrich III and D. Pines, J. Low Temp. Phys. 25, 673 and 691 (1976); See also David Pines, Lecture Notes in Phyiscs 198, Springer-Verlag 1984.

7. K.S. Singwi, M.P. Tosi, R. Land and A. Sjolander Phys. Rev. 176, 589 (1968).

8. K.S. Singwi and M.P. Tosi, Solid State Physics 36, 1981 Edited by H. Ehrenreich, F. Seitz and D. Turnbull (Academic press, New York).

9. P. Vashishta, R.K. Kalia and K.S. Singwi, in Electron-Hole Droplets in Semiconductors, edited by C.D. Jeffries and L.V. Keldysh (North-Holland, Amsterdam, 1983), P.1 and references therein.

10. J. Hansen, D. Levesque and D. Schiff, Phys. Rev. A. 3, 776 (1970).

11. C. DeDominicis and P.C. Martin, Phys. Rev. 105 1417 (1957).

12. V.N. Efimor and M.Ya. Amusia, Sov. Phys. (JETP) 20 388 (1965).

13. P. Vashishta and K.S. Singwi, Phys. Rev. B6, 875 (1972).

14. T.K. Ng and K.S. Singwi, to be published.

15. K. Skold and C.A. Pelizzari, Phil. Trans. Roy. Soc. Lond. B290 605 (1980).

16. C.H. Aldrich III and D. Pines, J. Low Temp. Phys. 32 689 (1978).

17. H.R. Glyde and F.C. Khanna, Can. J. Phys. 58, 343 (1980).

18. R.B. Hallock, J. Low Temp. Phys. 9, 109 (1972).

19. E.K. Achter and L. Meyer, Phys. Rev. 188, 291 (1969).

20. S. Fantoni and V.R. Pandharipande, Phys. Rev. Lett., 48, 178 (1982).

21. B.L. Friman and E. Krotscheck: Phys. Rev. Lett. 49, 1705 (1982).

22. G. Vignale and K.S. Singwi: Phys. Rev. B32, 2156 (1985).

23. D.N. Lowy and G.E. Brown, Phys. Rev. B12, 2138 (1975).

24. G.D. Mahan: Many-Particle Physics (Plenum 1981).

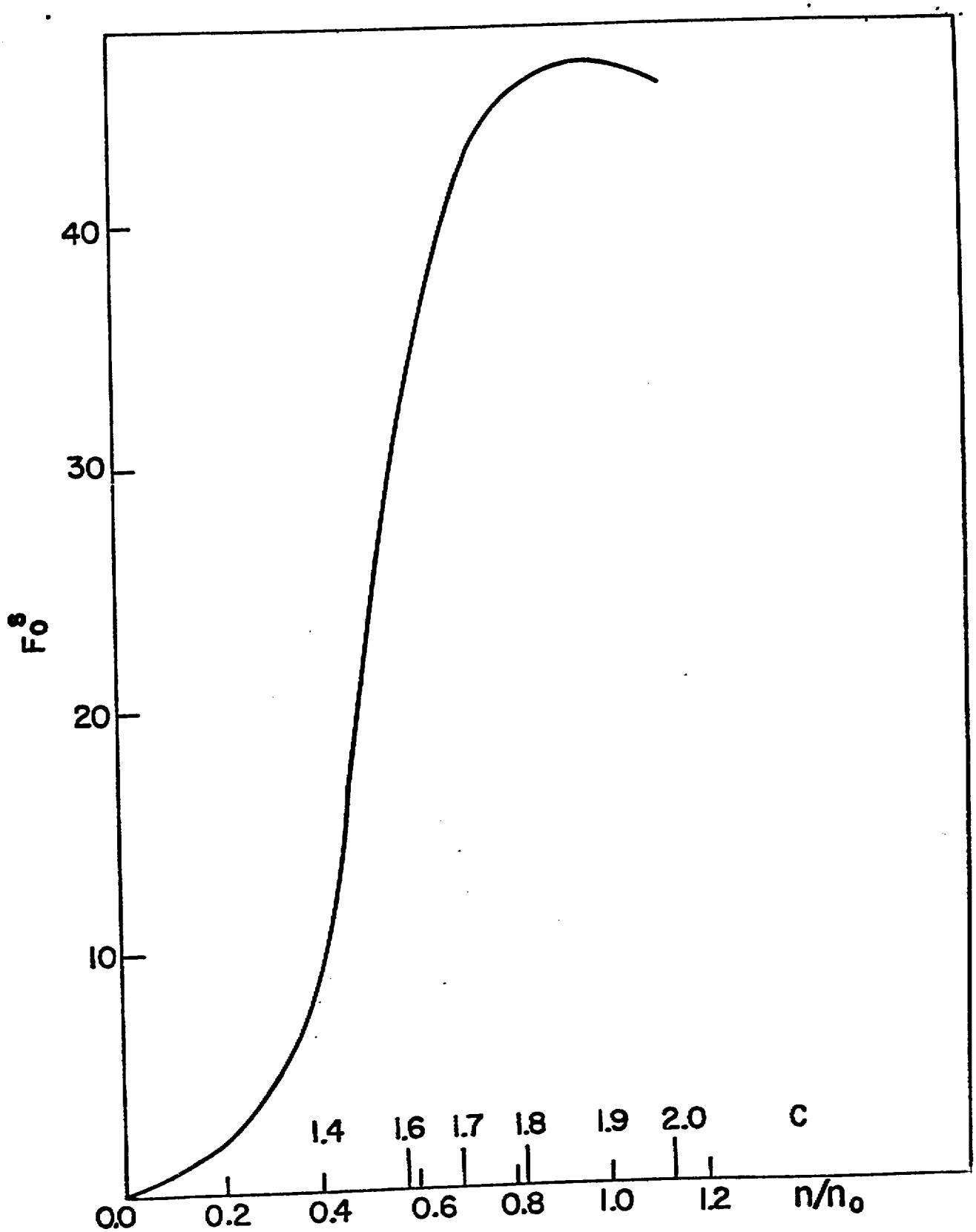

Fig. 1a

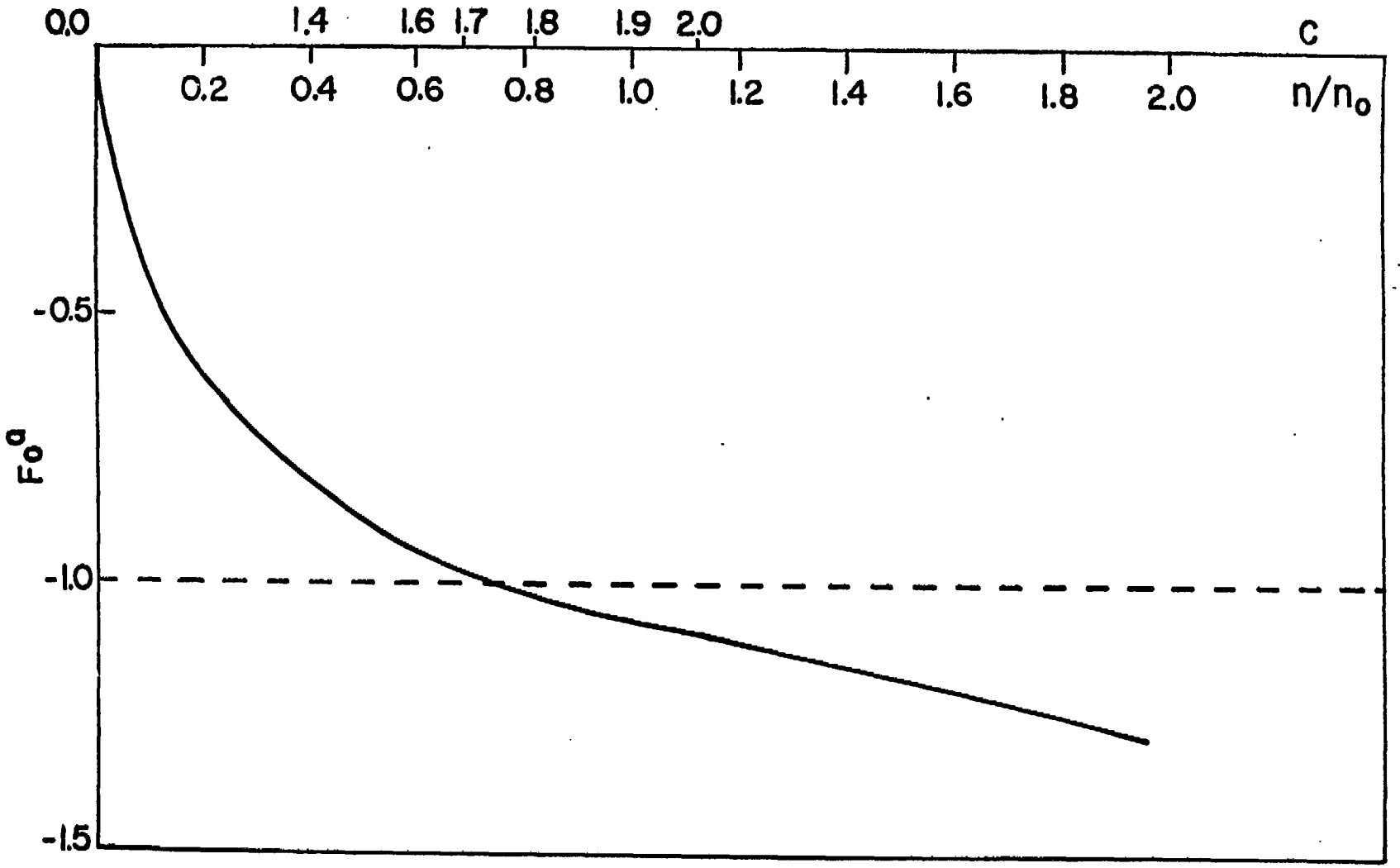

Fig. 1b

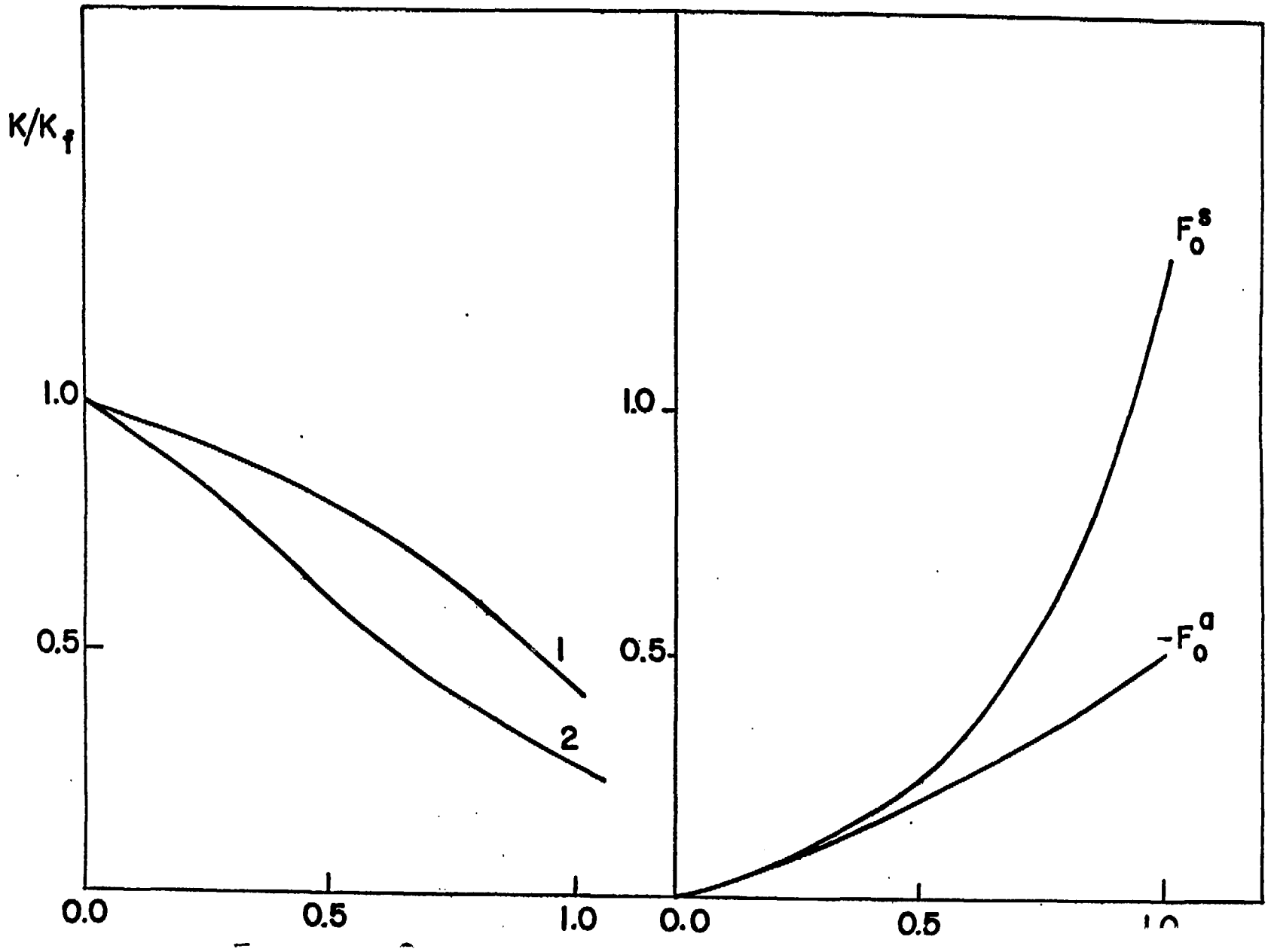
K/K_f
1.0
0.5
0.0
0.5
1.0
1
2
1.0
0.5
0.0
0.5
F_0^s
-F_0^a

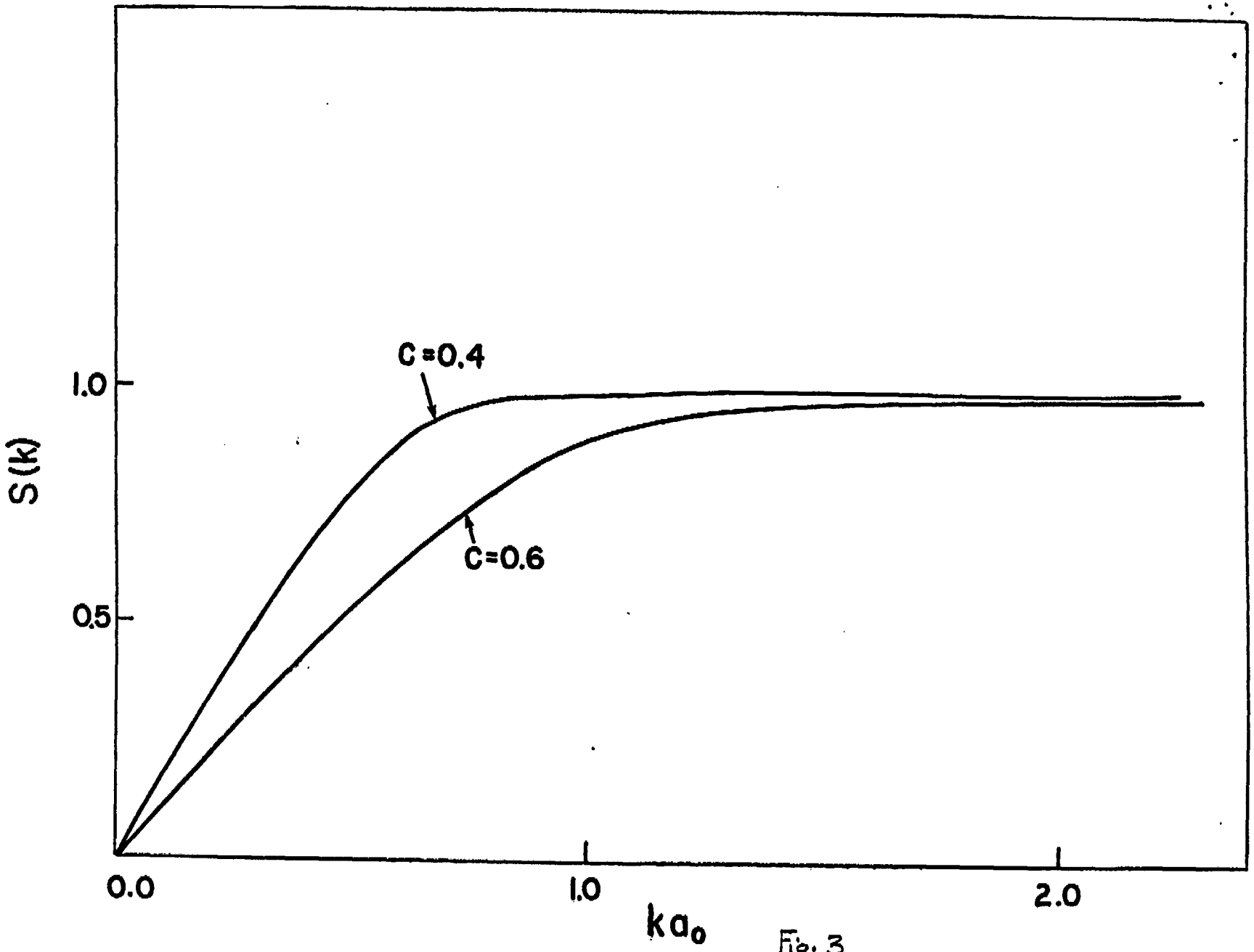

Fig. 3

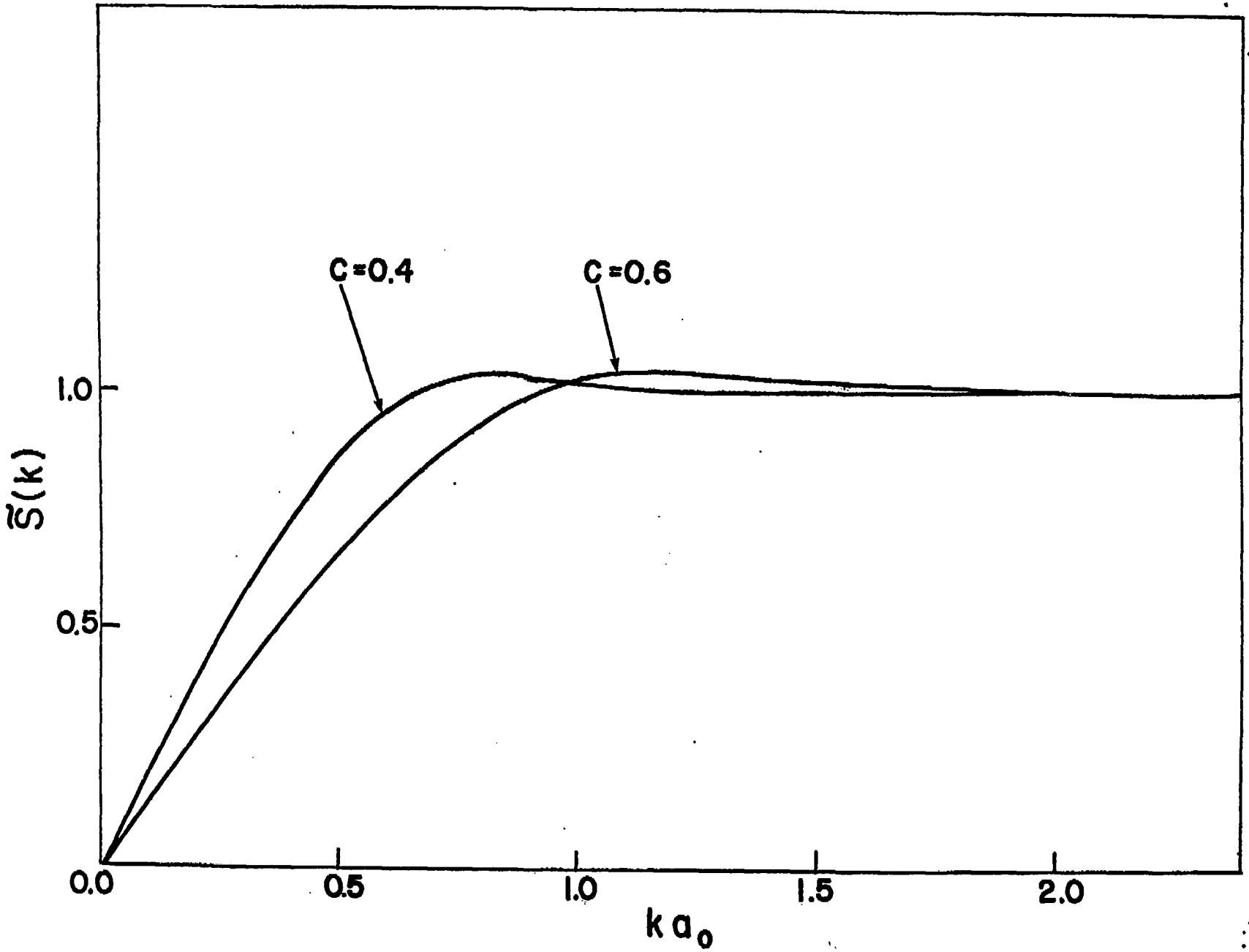
C=0.4
C=0.6
1.0
0.5
0.0
0.5
1.0
1.5
2.0
S̃(k)
k a₀

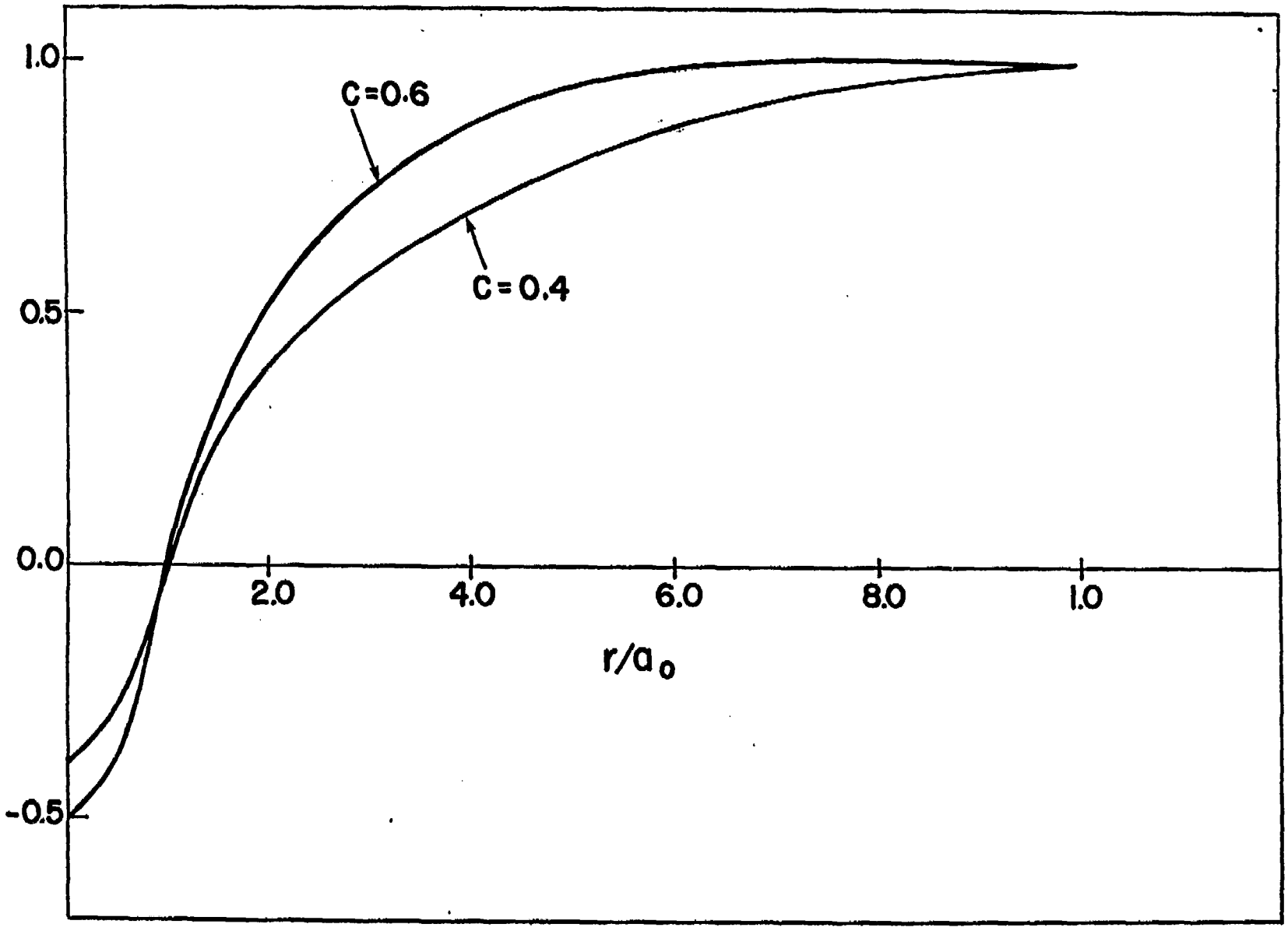

Fig. 5

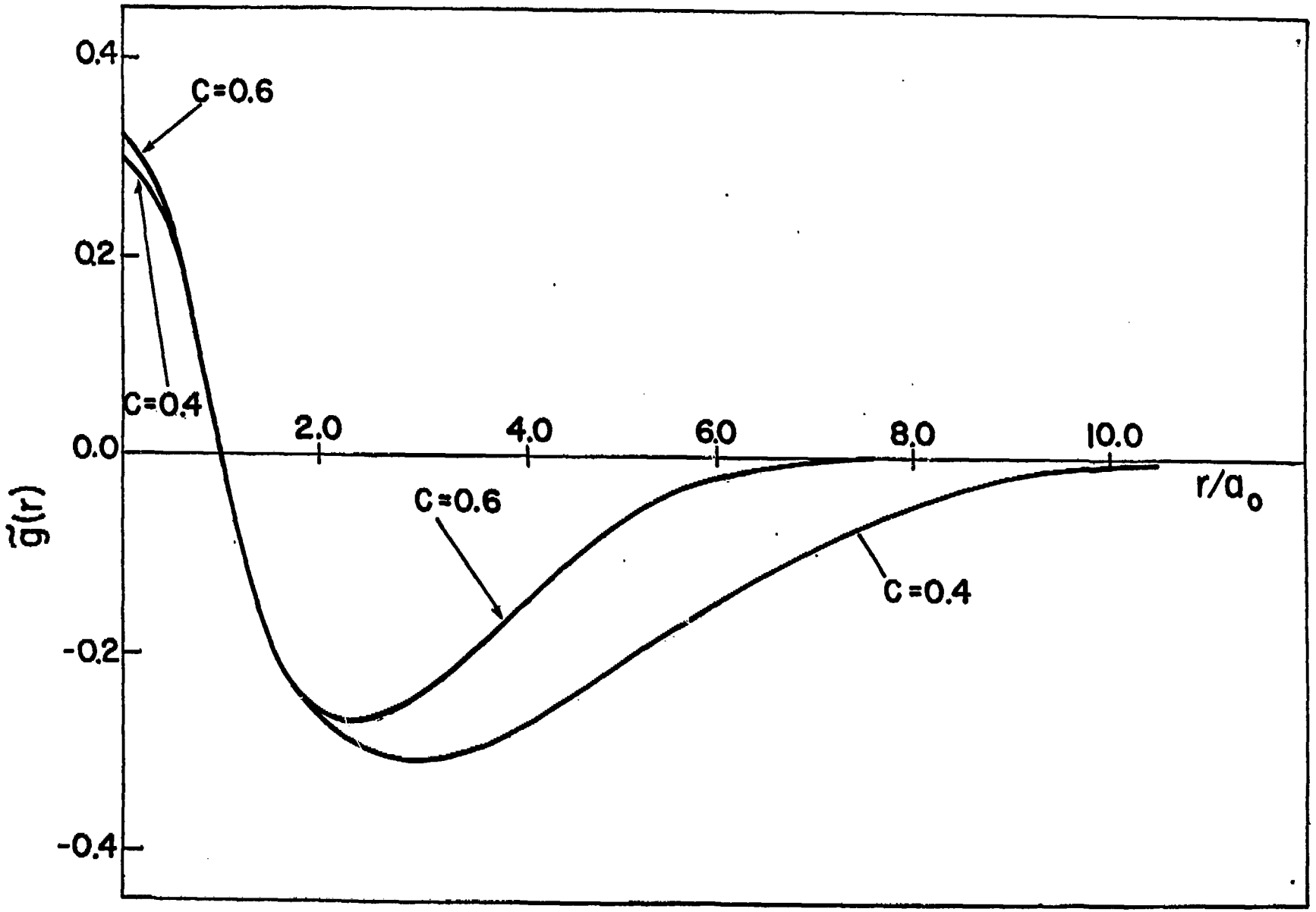

Fig. 6

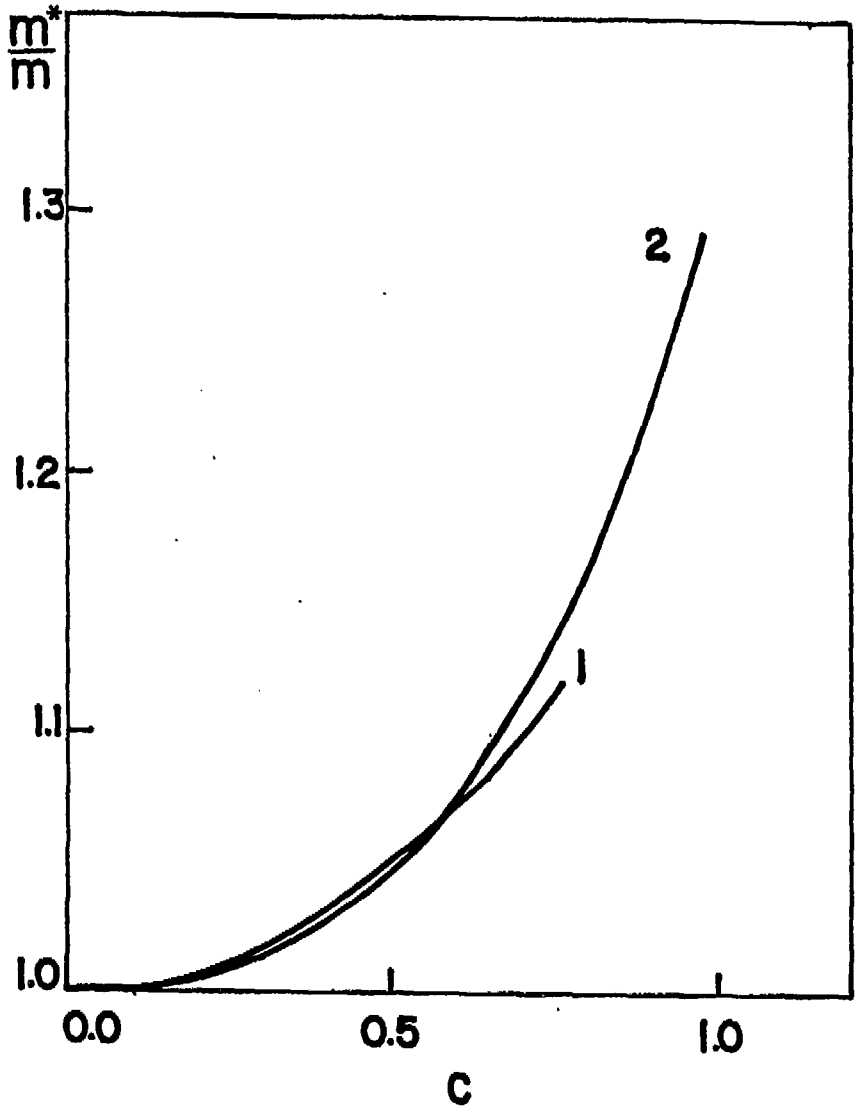

Fig. 7

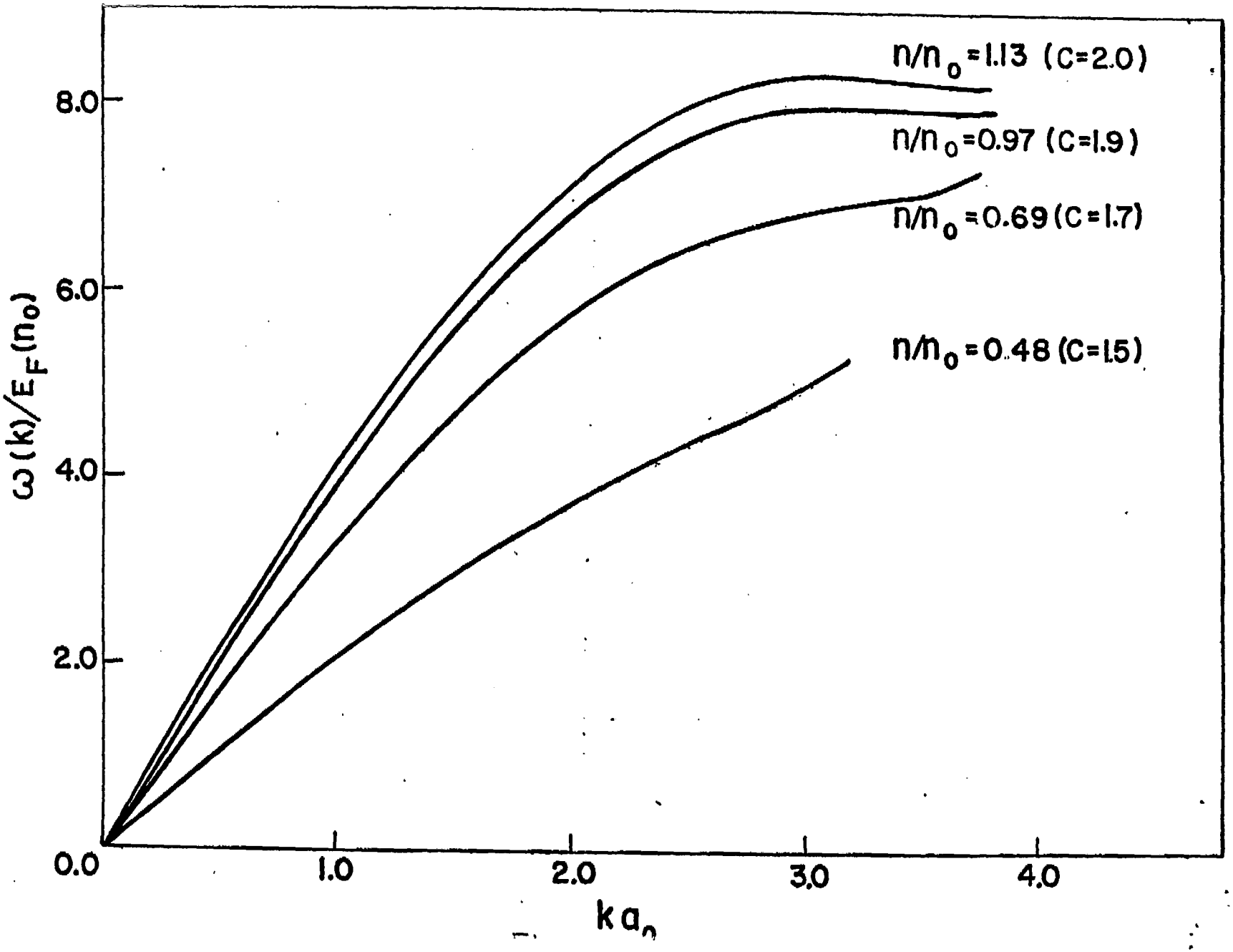
$n/n_0 = 1.13$ (C=2.0)
$n/n_0 = 0.97$ (C=1.9)
$n/n_0 = 0.69$ (C=1.7)
$n/n_0 = 0.48$ (C=1.5)
$\omega(k)/E_F(n_0)$
8.0
6.0
4.0
2.0
0.0
1.0
2.0
3.0
4.0
ka_n

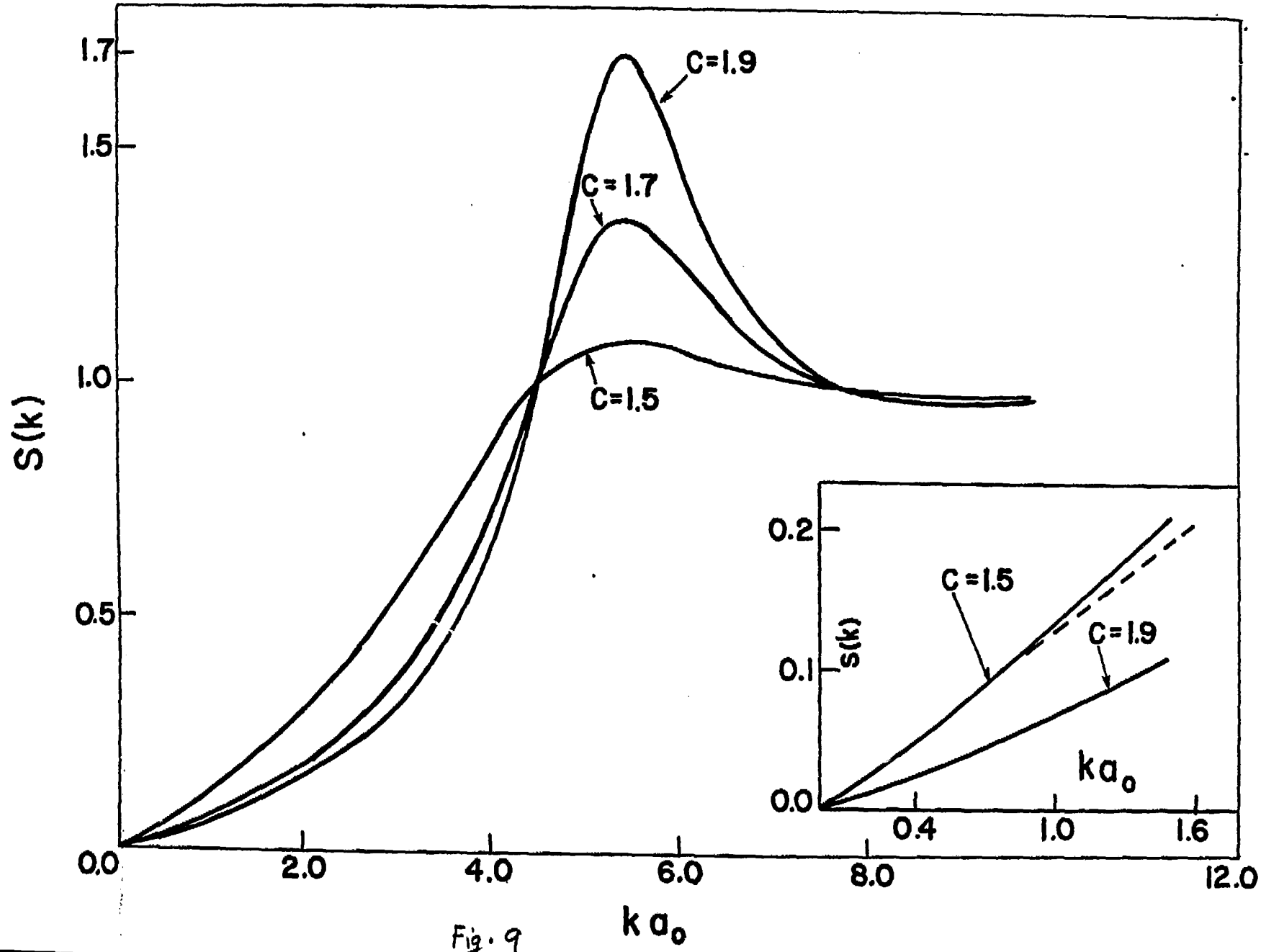
1.7
1.5
1.0
0.5
0.0
S(k)
C=1.9
C=1.7
C=1.5
2.0
4.0
6.0
8.0
12.0
k a₀
0.2
0.1
0.0
S(k)
C=1.5
C=1.9
ka₀
0.4
1.0
1.6

Fig. 9

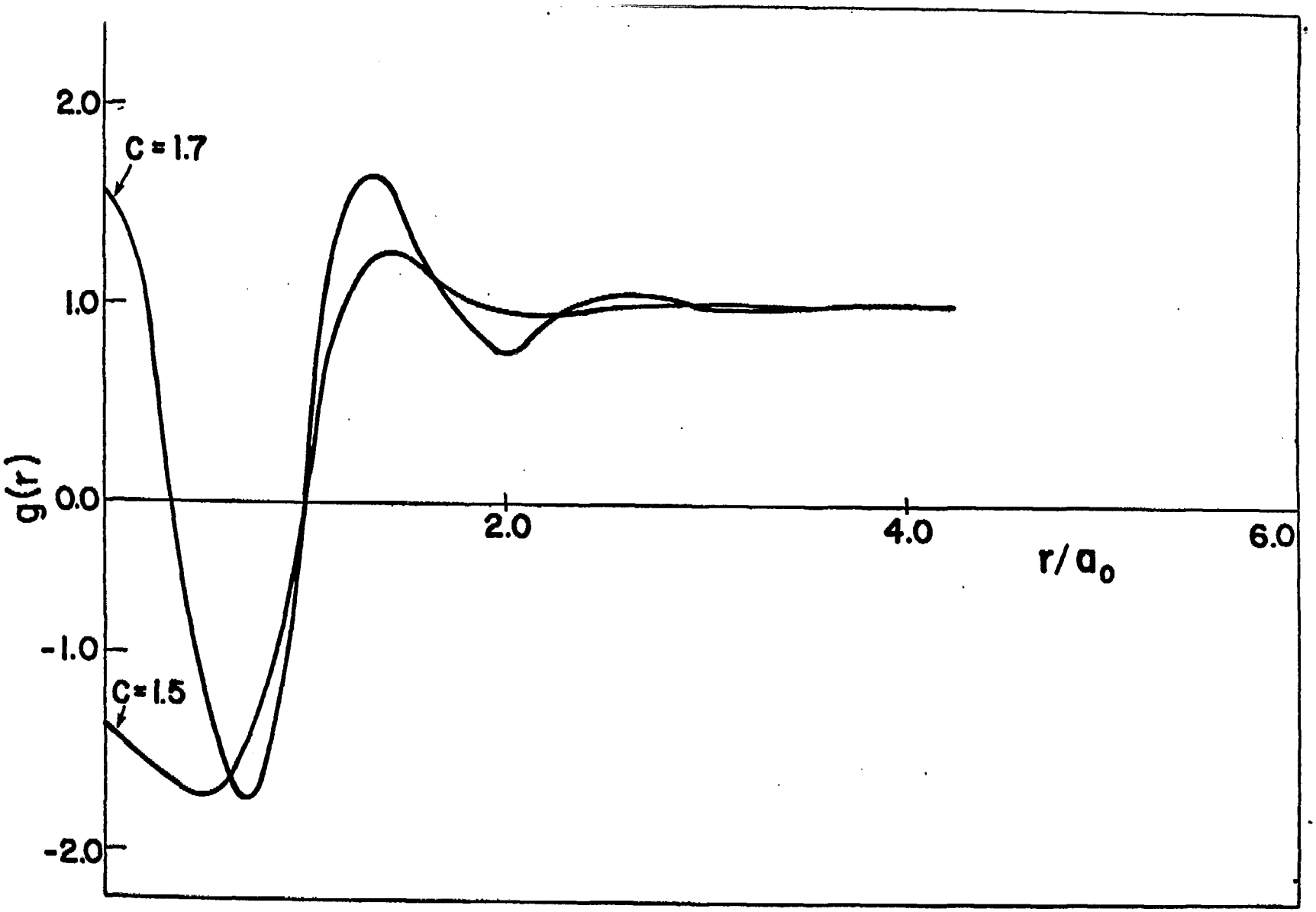

Fig. 10

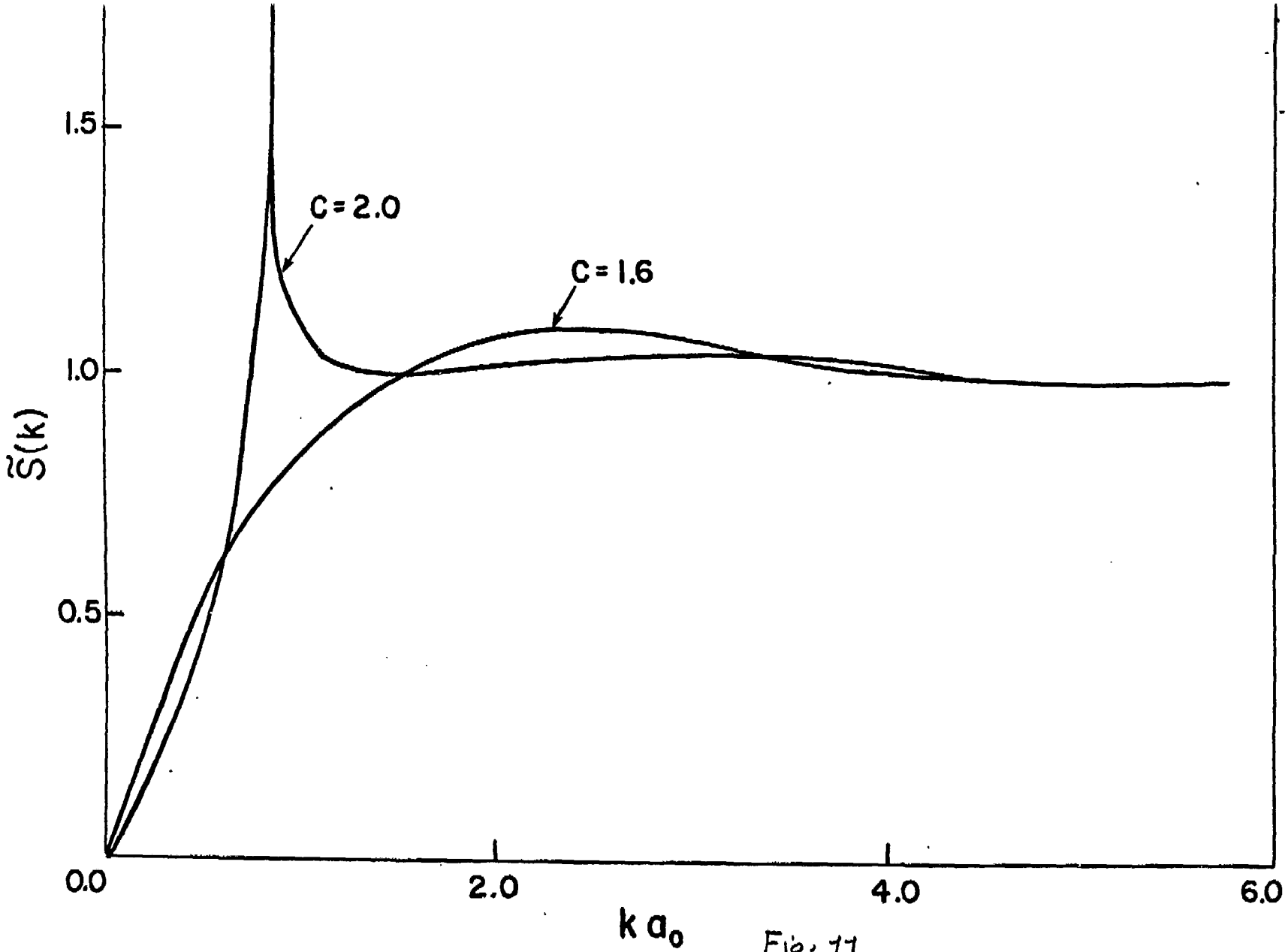

Fig. 11

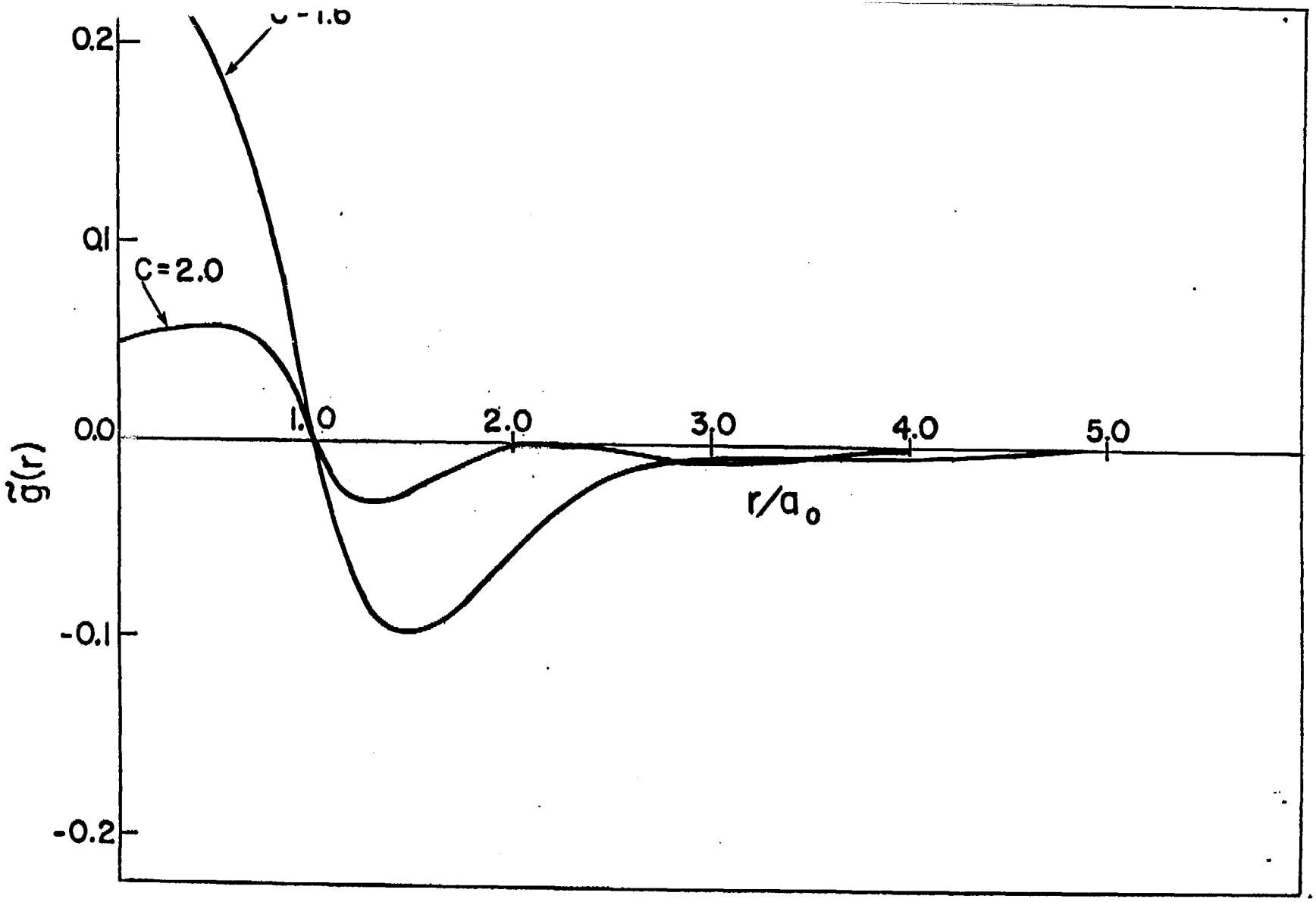

Fig. 12

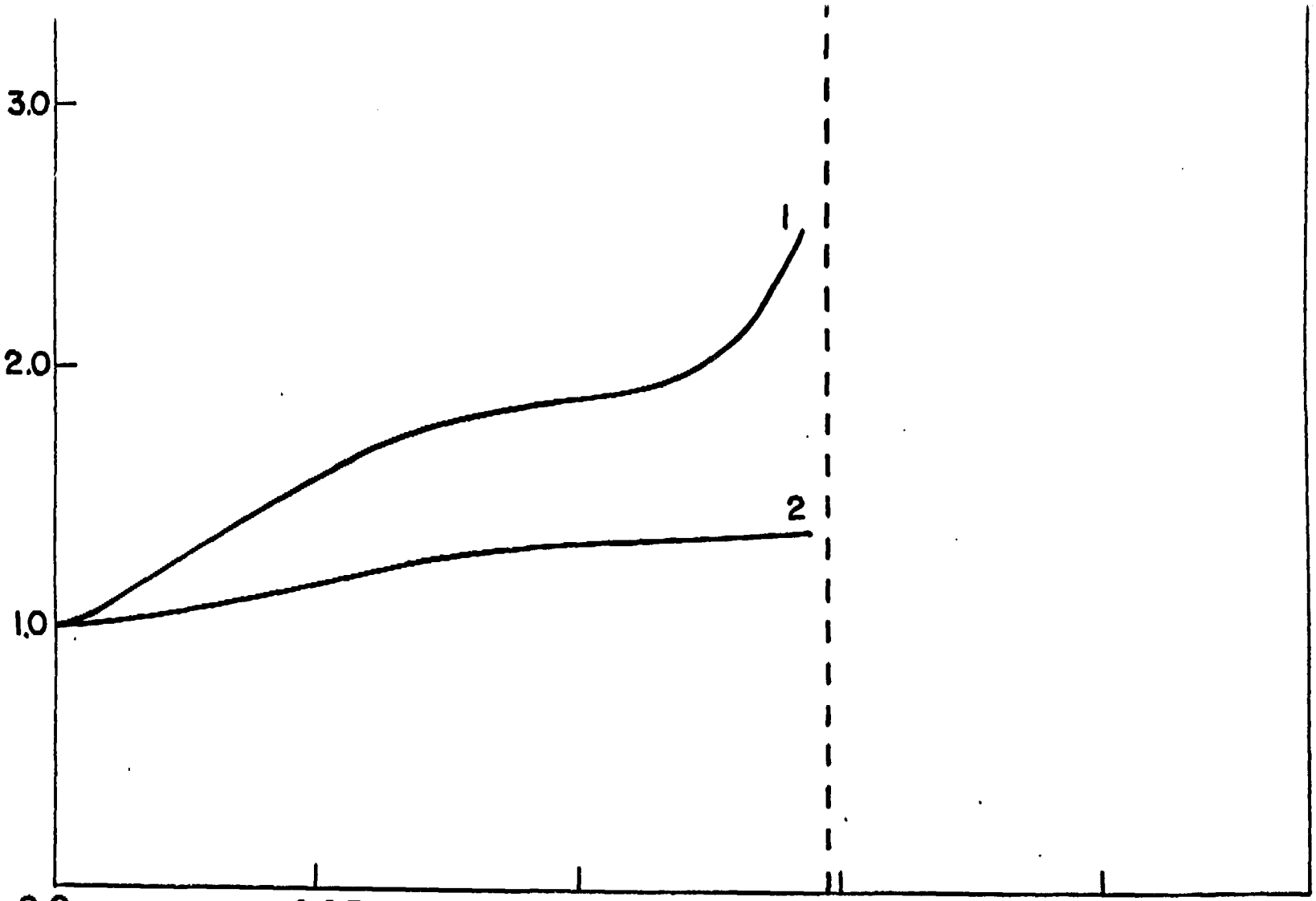

Fig. 13

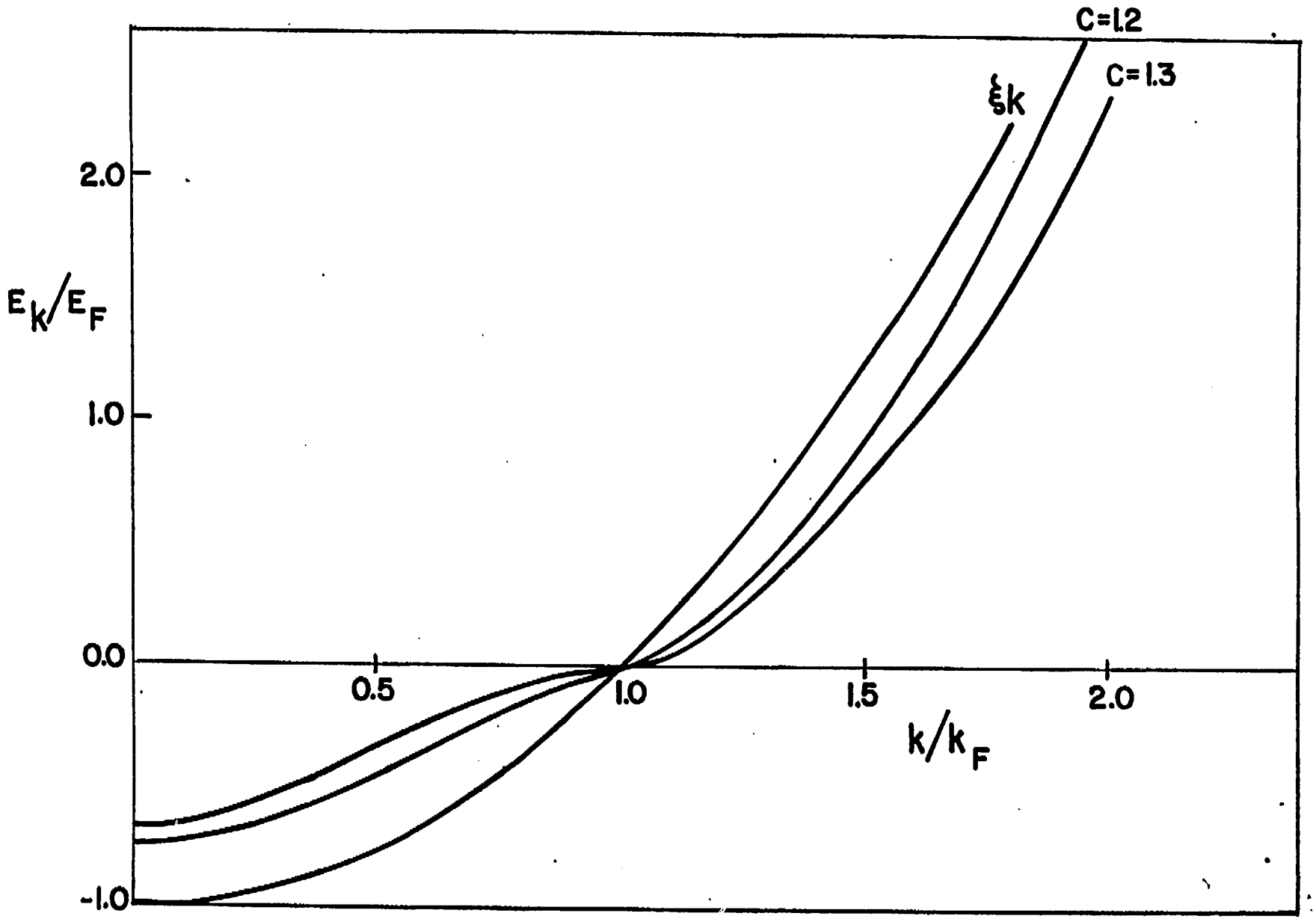

Fig. 14

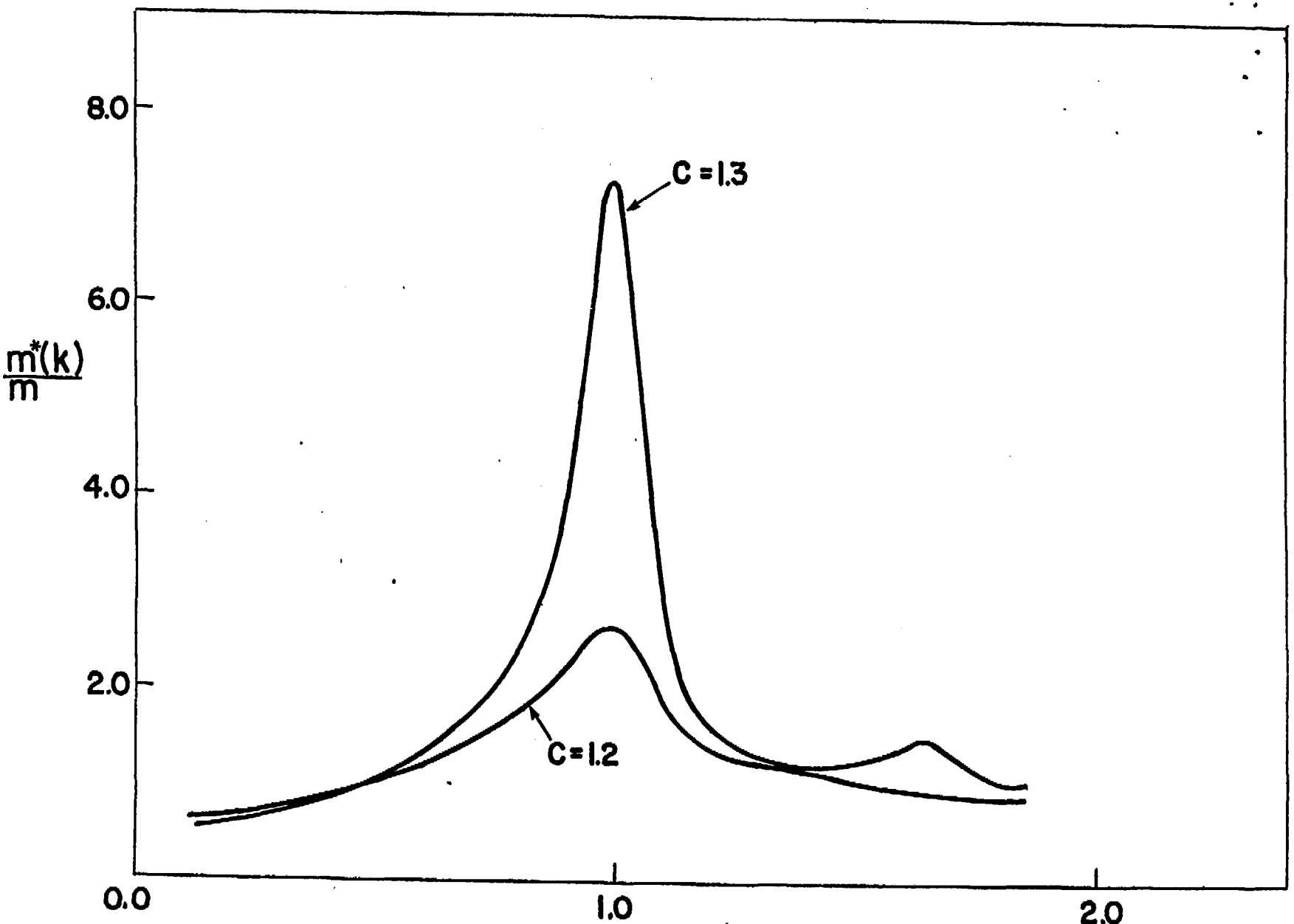

Fig. 15

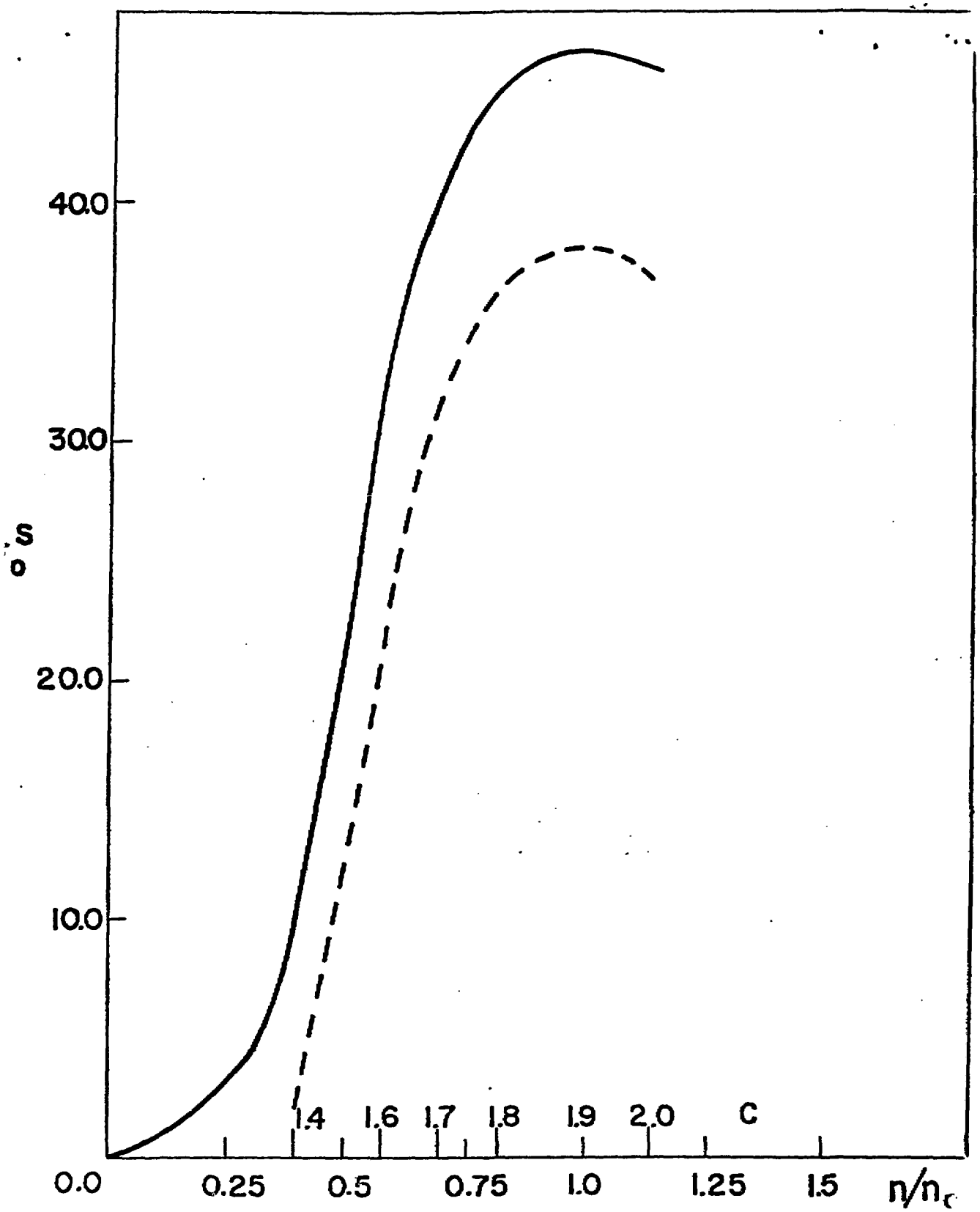

Fig. 16

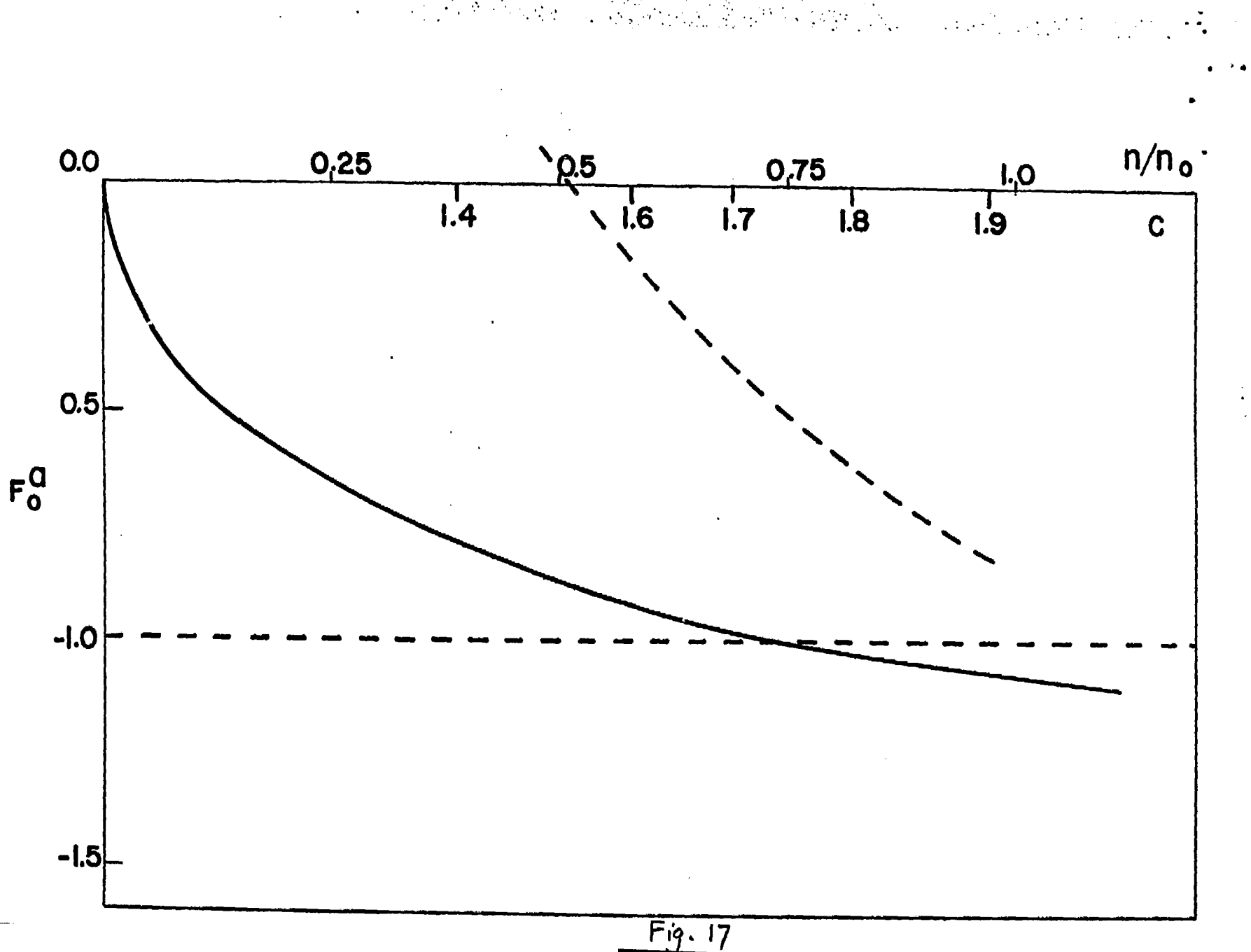

Fig. 17

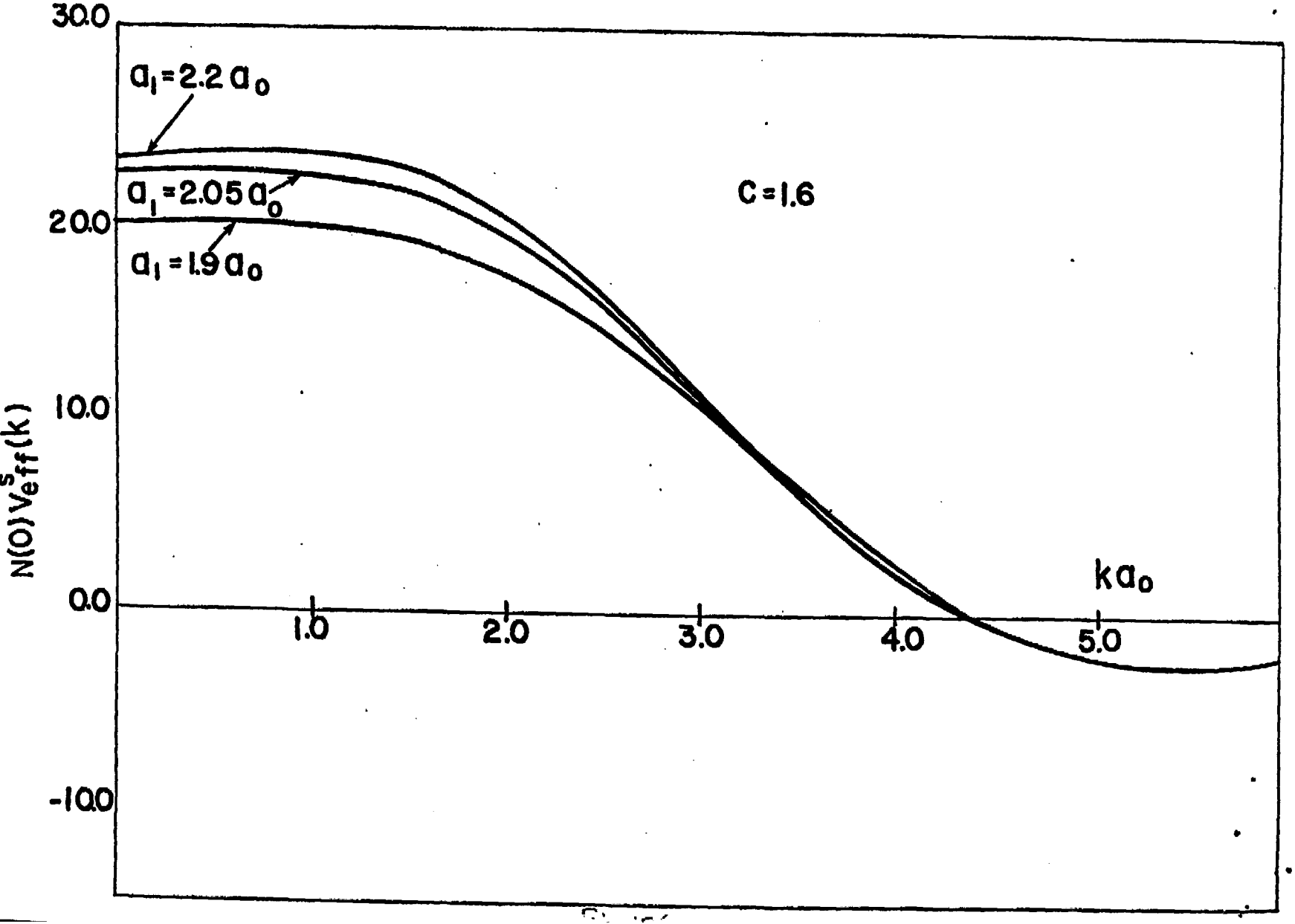
30.0
20.0
10.0
0.0
-10.0
$a_1 = 2.2\,a_0$
$a_1 = 2.05\,a_0$
$a_1 = 1.9\,a_0$
C = 1.6
$N(0)V_{eff}^{S}(k)$
ka_0
1.0
2.0
3.0
4.0
5.0

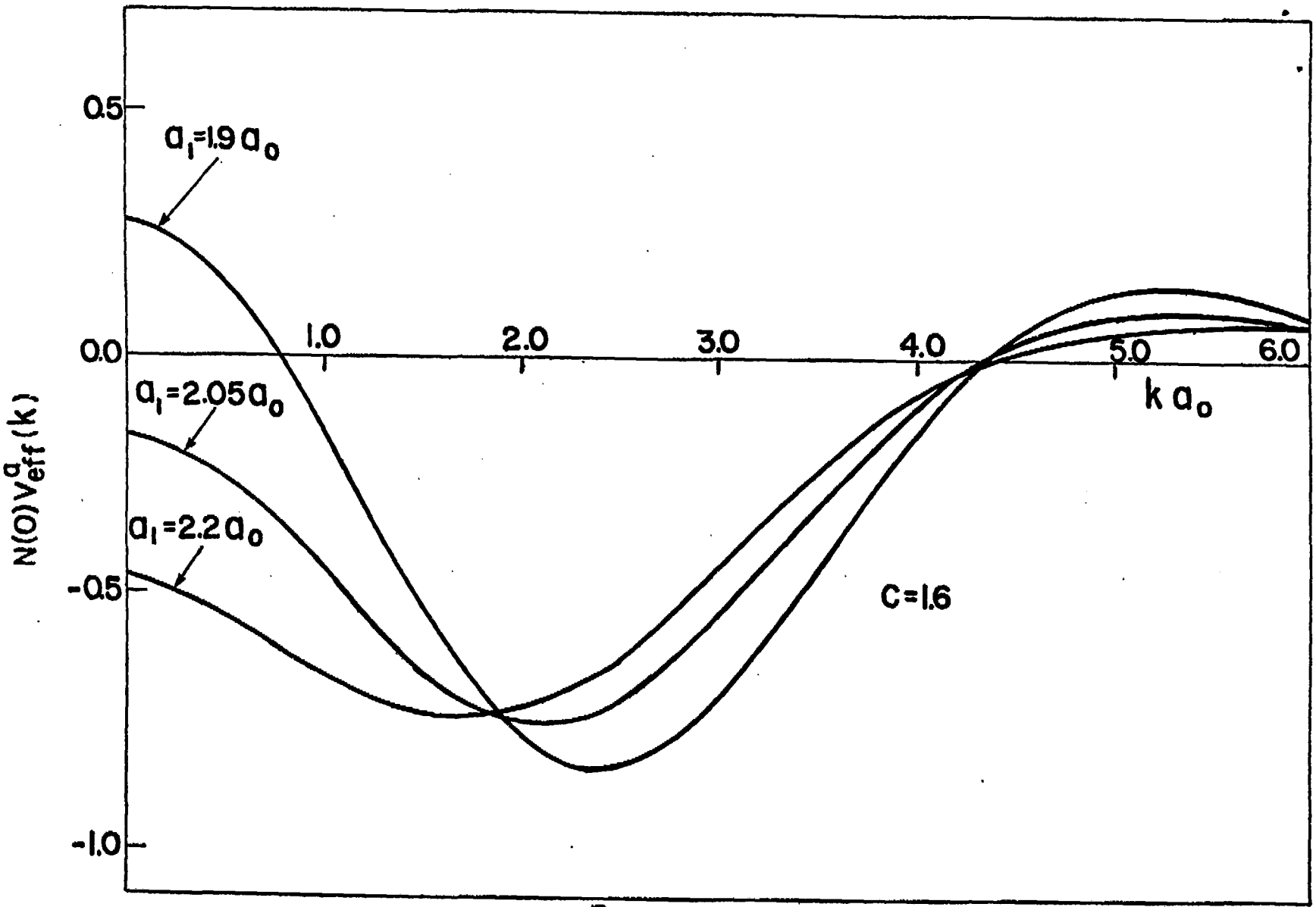
0.5
0.0
-0.5
-1.0
1.0
2.0
3.0
4.0
5.0
6.0
k a_o
N(0)V_eff^a(k)
a_1=1.9 a_o
a_1=2.05 a_o
a_1=2.2 a_o
C=1.6

Fig. 19

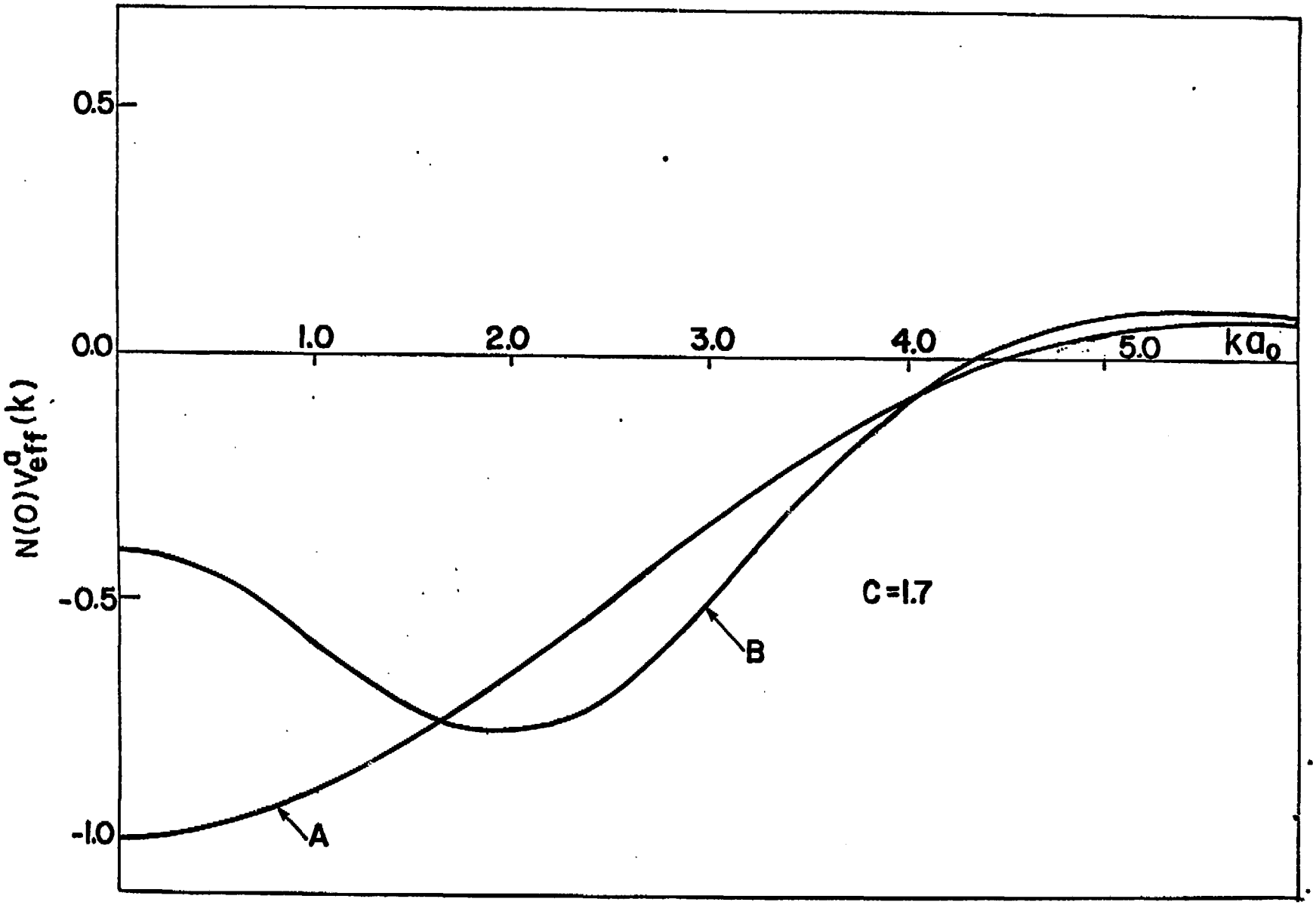

Fig. 2.a

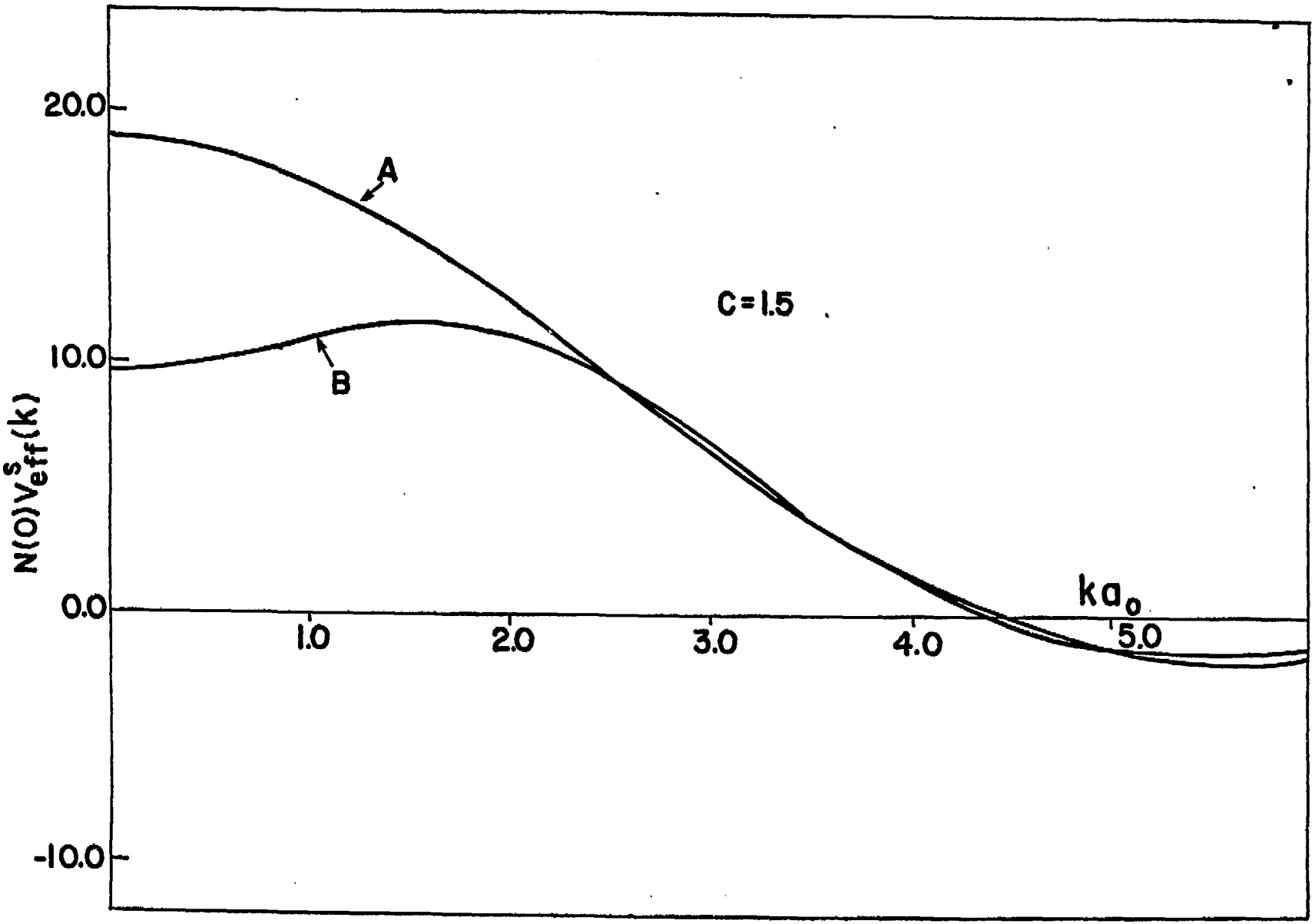

Fig. 21

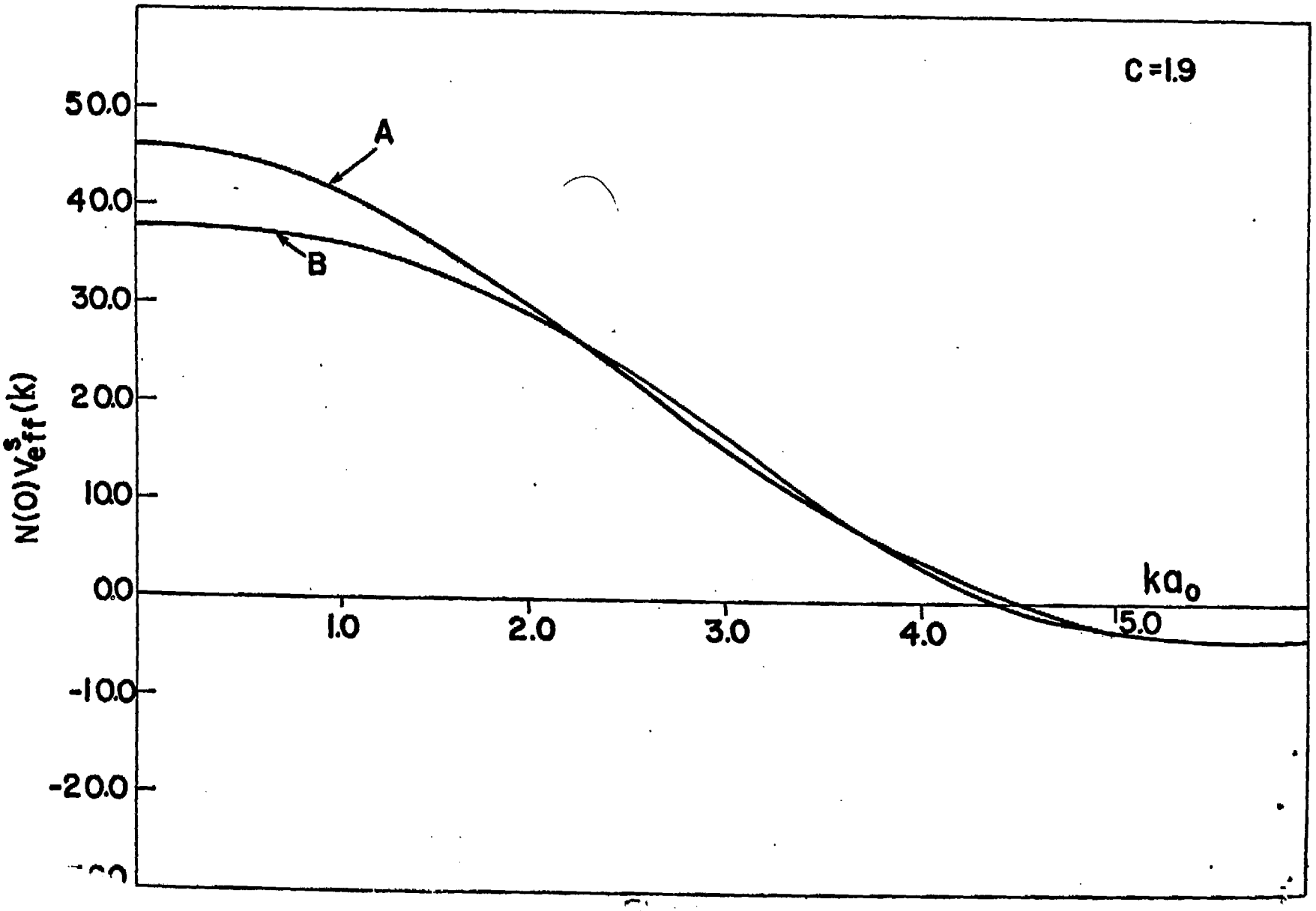
C=1.9
A
B
50.0
40.0
30.0
20.0
10.0
0.0
-10.0
-20.0
N(0)V$^s_{eff}$(k)
1.0
2.0
3.0
4.0
5.0
ka$_0$

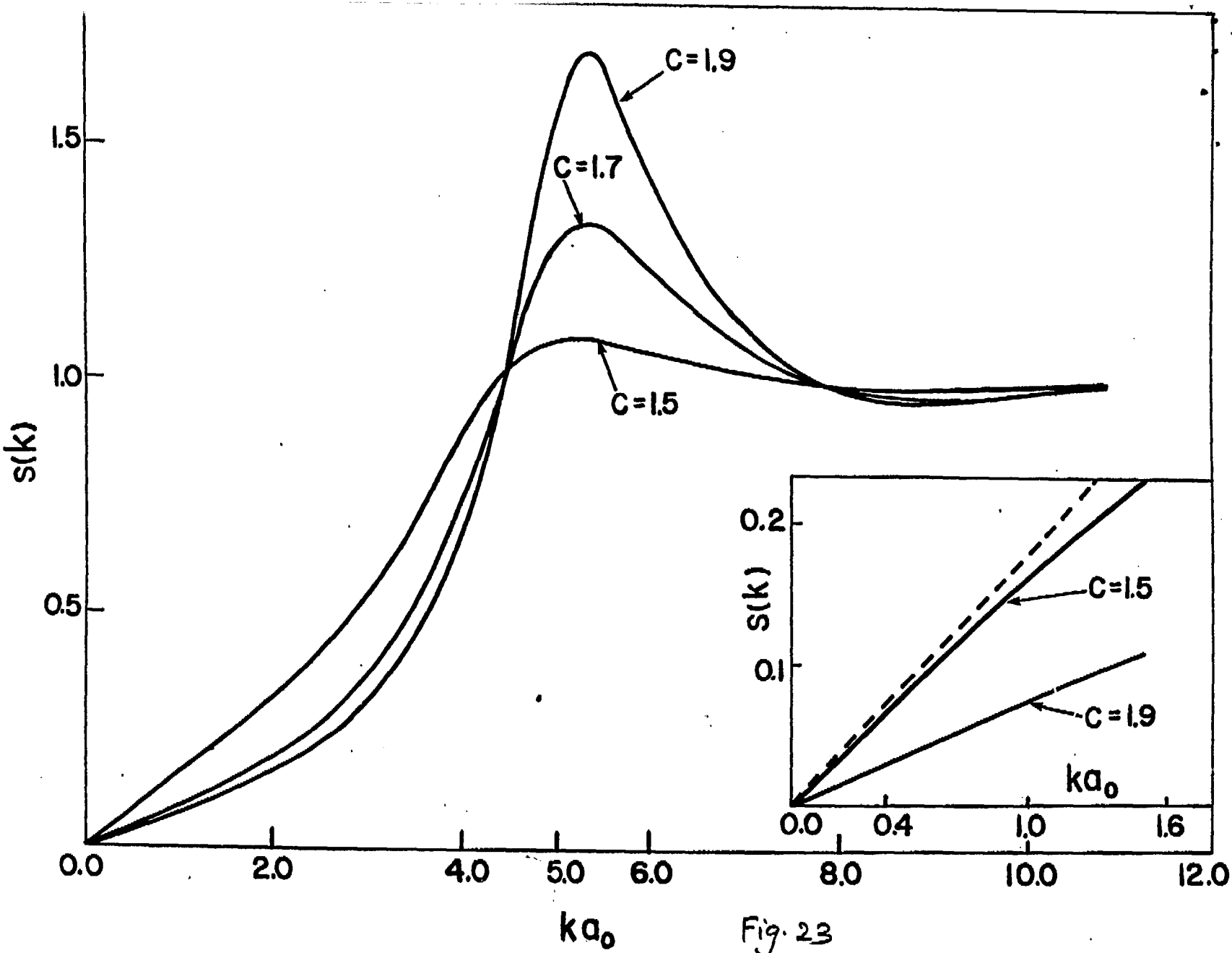
C=1.9
C=1.7
C=1.5
s(k)
1.5
1.0
0.5
0.0
2.0
4.0
5.0
6.0
8.0
10.0
12.0
ka0
0.2
0.1
C=1.5
C=1.9
ka0
0.0
0.4
1.0
1.6

Fig. 23

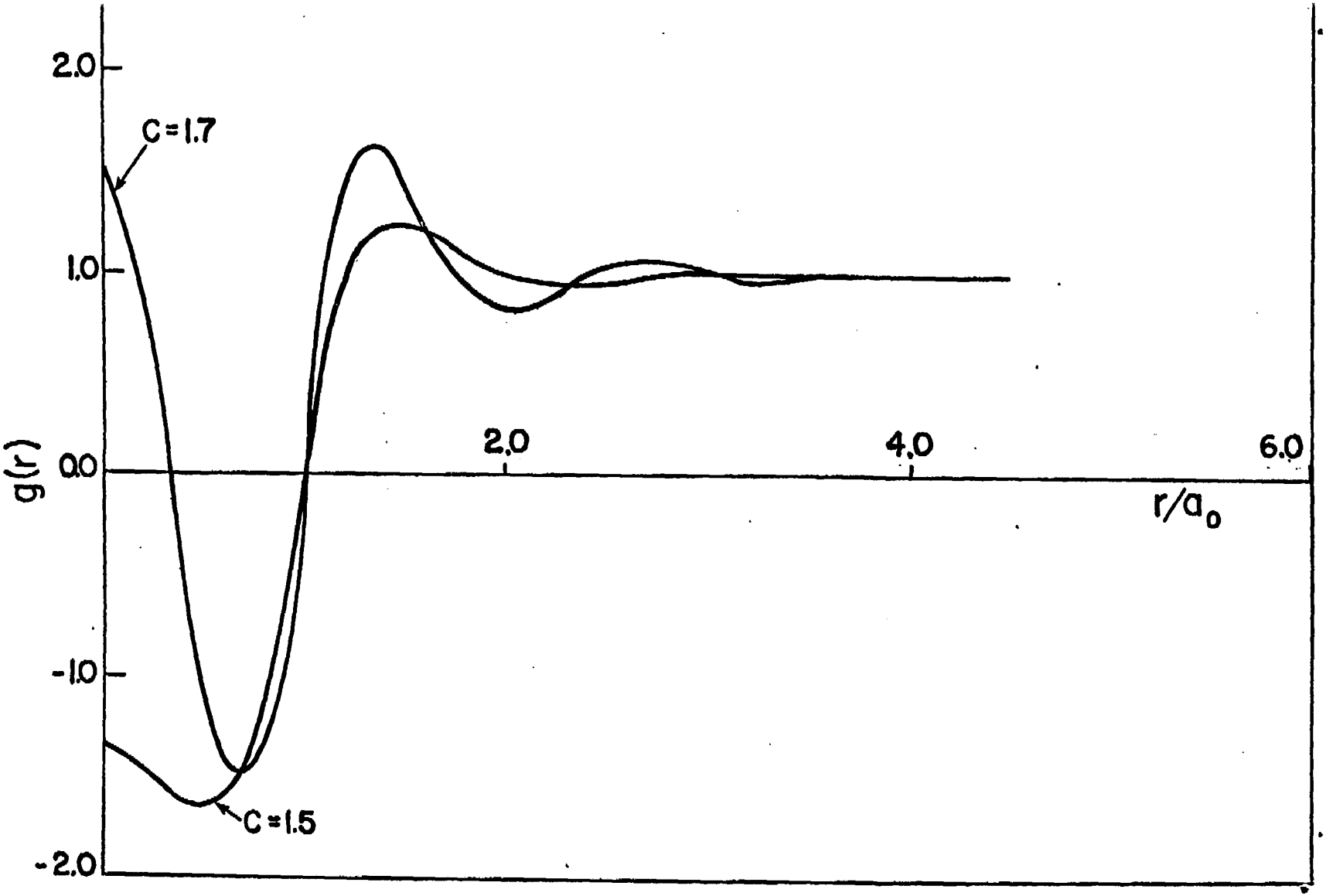

Fig. 24

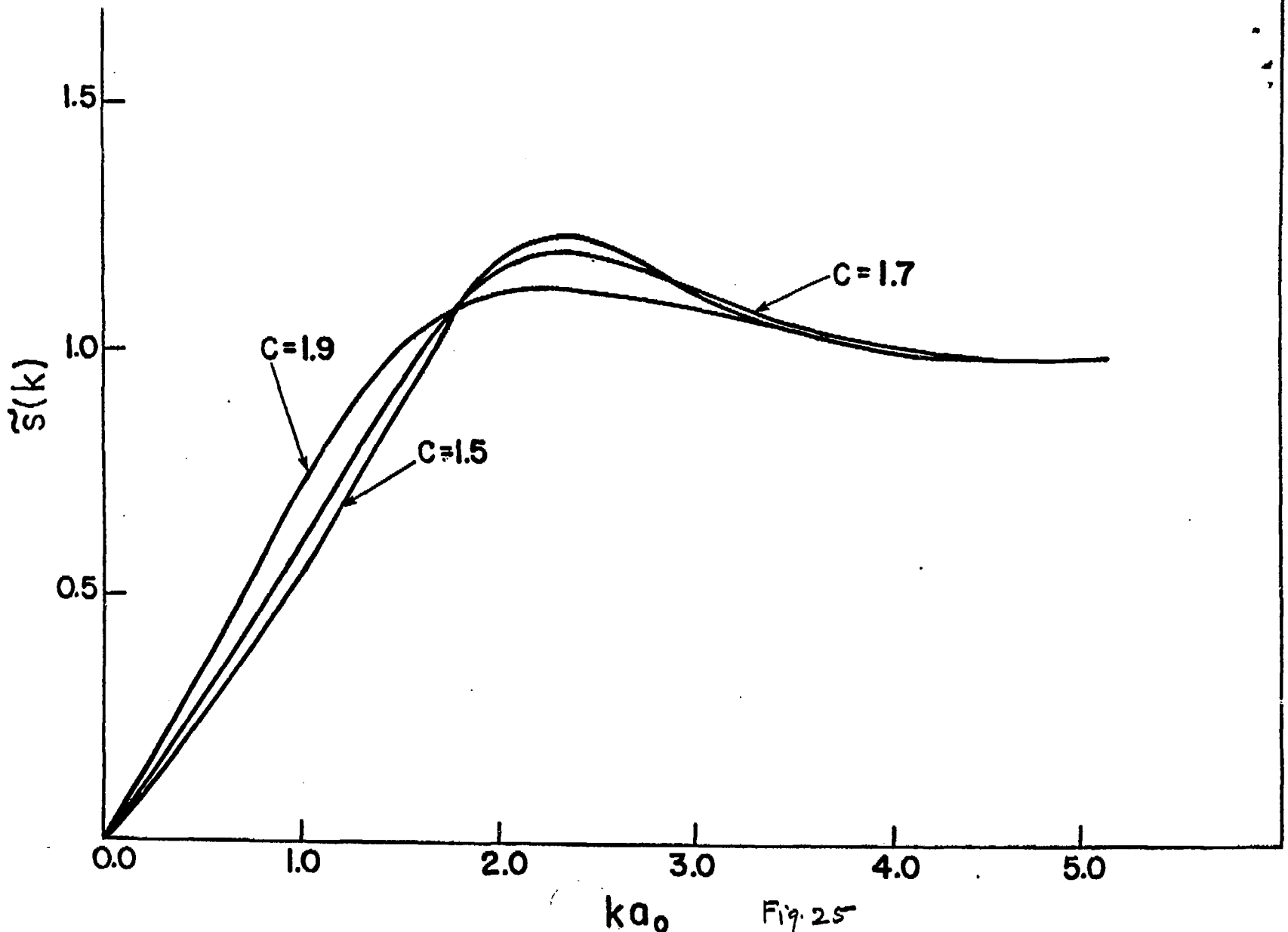

Fig. 25

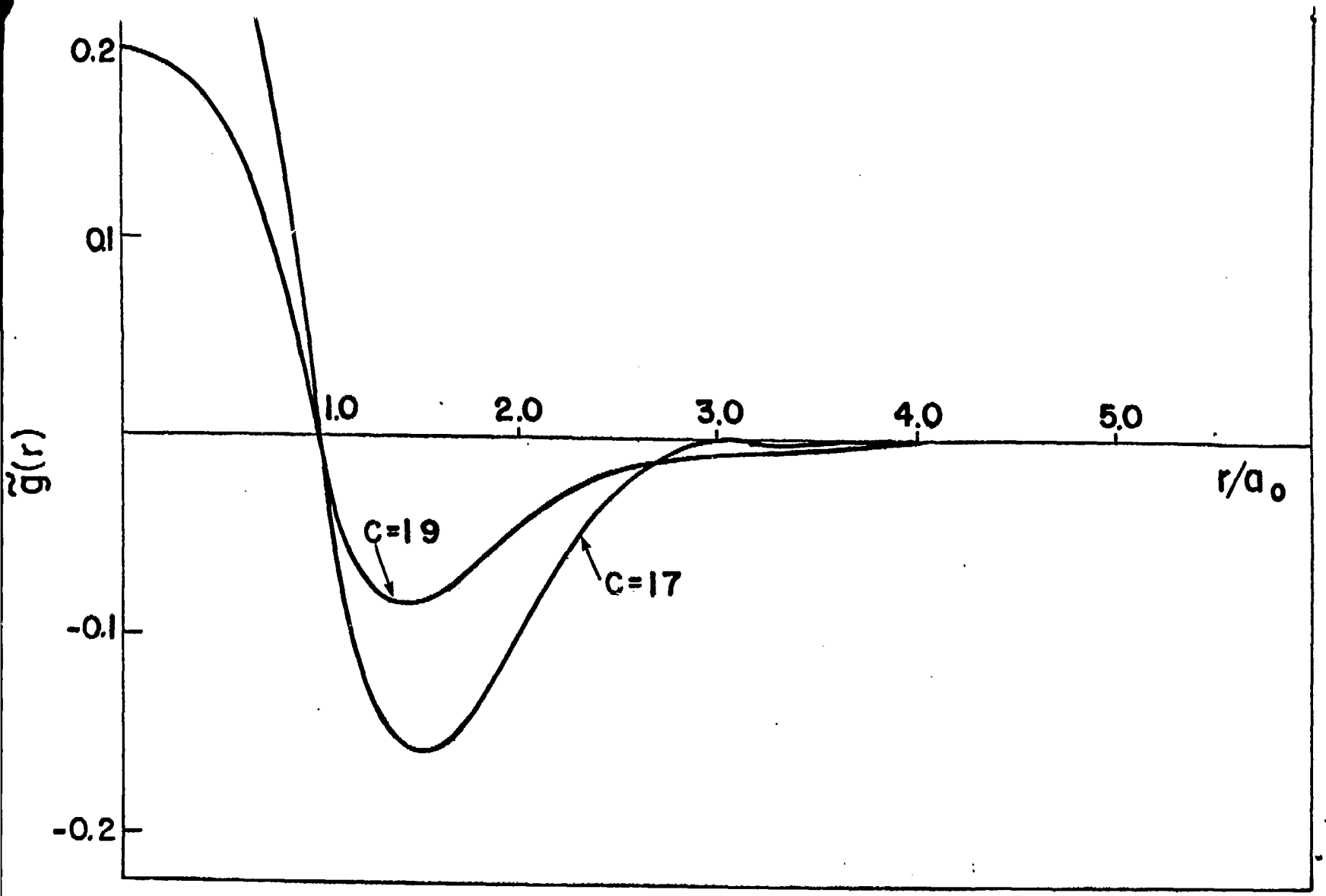

Fig. 26

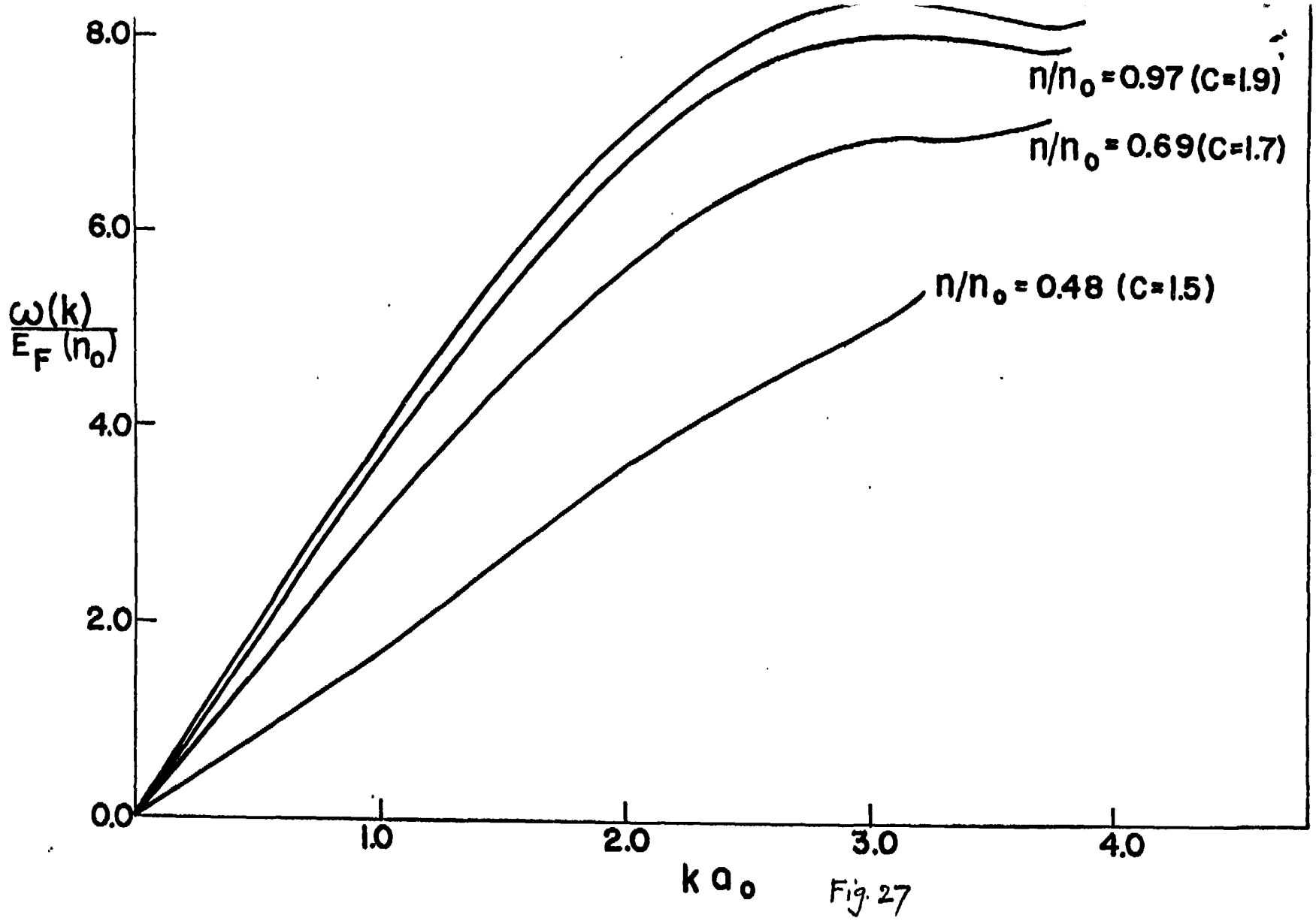
8.0
6.0
4.0
2.0
0.0
$\frac{\omega(k)}{E_F(n_0)}$
$n/n_0 = 0.97$ (C=1.9)
$n/n_0 = 0.69$ (C=1.7)
$n/n_0 = 0.48$ (C=1.5)
1.0
2.0
3.0
4.0
$k a_0$

Fig. 27

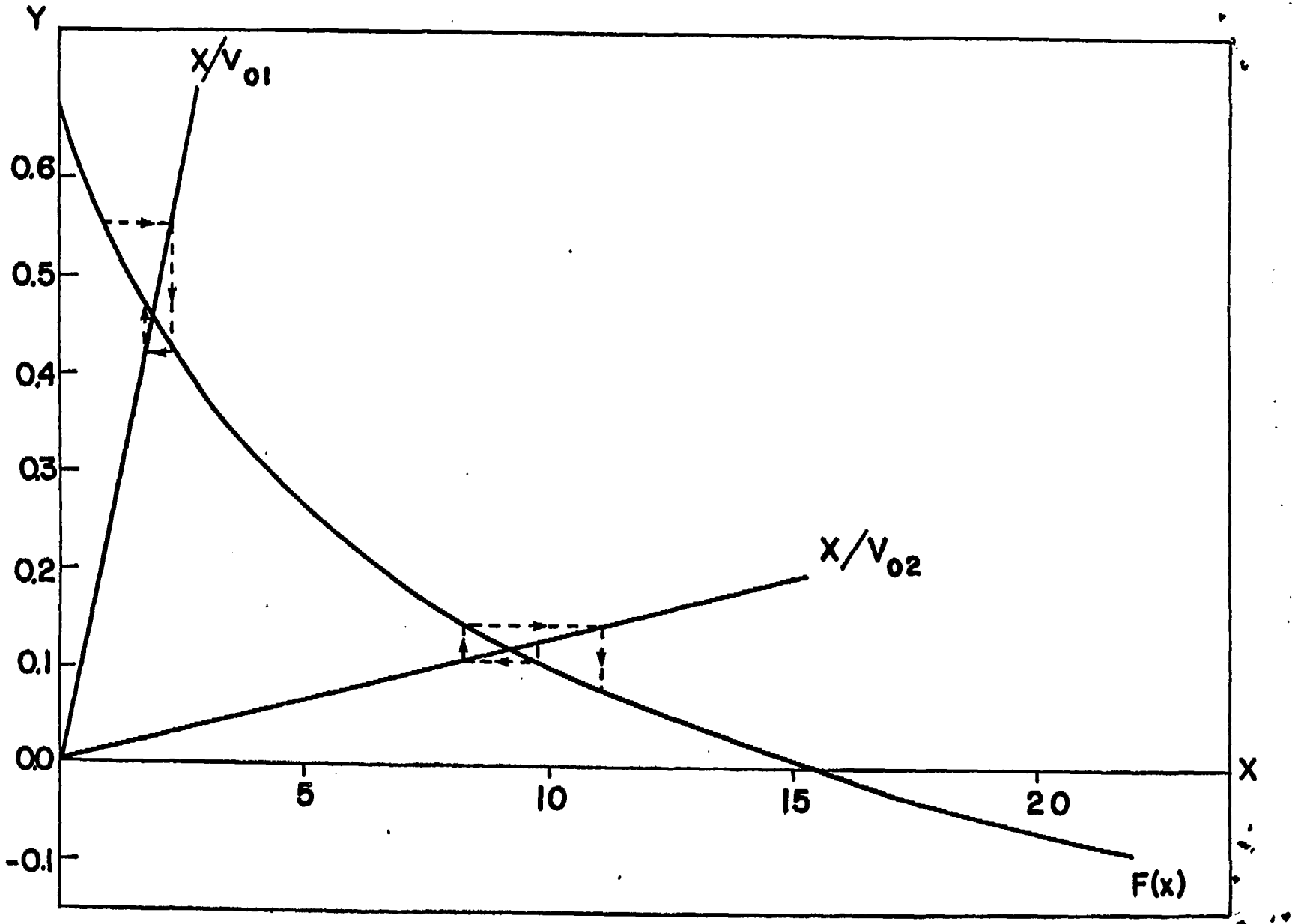

Fig. 28